Development of Spreading Algorithms for the ROC

by

J. A. Galt and Roy Overstreet

Genwest Systems, Inc.

Acknowledgements:

Funding for the Response Options Calculator (ROC) has been provided by:

Shell Oil Co. - Contract 4600004618. Contact Victoria Broje 281-544-7437

Minerals Management Service of the U.S. Department of the Interior – Contract M08PX20200. Contact Joseph Mullin 703-787-1556

American Petroleum Institute – Contracts 2008-103625 & 2009-104117. Contact Marc Hodges 202-682-8146

Introduction:

This study describes a mechanically based spreading algorithm. It is intended as a heuristic simulation to be used in conjunction with an oil weathering model. Initially this will support a set of routines to describe and quantify oil spill recovery options. The immediate target application is the ROC development project that includes routines to look at mechanical cleanup, dispersant use and burning as recovery/treatment methods. By "heuristic" we mean that the routines will be practical and described by simple scenario parameters that will typically be available for all cases. It will be a simulation in the sense that it will produce results that correspond to the observed behavior of real slicks, but will not necessarily try to describe the detailed dynamics of the physical processes involved.

The algorithms presented here are intended to modify standard spreading routines that describe a single contiguous slick. The primary goal is to provide estimates of differential thickness information corresponding to observations of real slicks and is associated with "oil droplet" formation due to wave action and "Langmuir" cells. These algorithms are formulated in such a way that they can be used as correction factors to any oil-weathering/spreading model that is assumed to preserve the mass balance of the slick.

The first segment of this study focuses on droplet formation, the second on Langmuir cells.

Section One

1.0 - Droplet Model:

For oil slicks it is very common to see the formation of a "comet" shape with the thicker portion of the slick forming on the downwind edge.

Figure 1 –

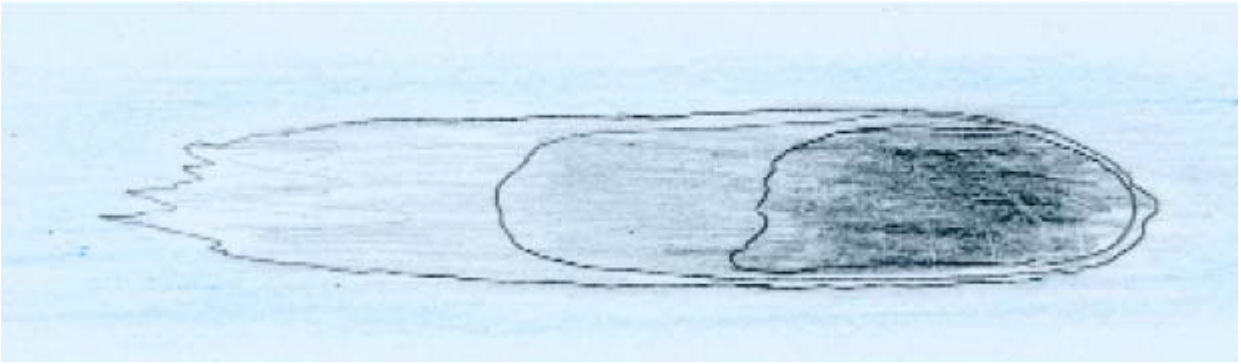

Our first task will be to formulate a simple process that can explain this behavior and develop an algorithm to describe it. A good starting point is the work done by Delvigne on the formulation of oil droplets from a slick subjected to various forms of turbulence. Dr. Delvigne has published a number of papers on the subject, but the summary, Delvigne(1993), gives a good basis for what we would like to develop and for this study will be referenced simply as "Delvigne".

Figure 2 –

Figure 2 shown above gives a general picture of the process that we wish to encapsulate in this section of the algorithm. Basically it is hypothesized that: (1) Wave action breaks a contiguous slick into droplets and mixes them below the surface. The droplet size distribution is known and ranges from quite small (fractions of a mm) to an upper limit that depends on the original thickness of the oil slick and the energy that is available for mixing. (2) The oil droplets that are submerged in this process continue to disperse, but they are typically buoyant and will rise back towards the surface. How fast they rise depends on their size, with the larger droplets resurfacing more quickly than the smaller ones. (3) Over the depth zone where the oil droplets are initially mixed there is a vertical shear in the horizontal currents due to the same wind and wave activity that supplies the original energy for the droplet formation. And finally (4) The larger droplets that rise quickly spend proportionally more time in the stronger currents near the surface, and subsequently move more rapidly downwind. The smaller droplets surface behind their larger cohorts and form the tail of the "comet-like" distribution shown in Figure 1. Some droplets will be so small that their buoyant velocities cannot overcome the turbulent dispersion processes and effectively never return to the surface which represents a loss term in the mass balance of the slick referred to as

"natural dispersion". Other droplets will be so large that their buoyant velocities insure that they are virtually never below the surface. We will now consider these physical processes in more detail starting with wave mixing.

1.1 Droplet Mixing Energy:

To put these hypothetical processes into algorithmic form we start off by following Delvigne who gives a formula for the fractional area of breaking waves which are thought to be the major turbulence source for droplet formation. (Delvigne, eq. 4)

$$F = \frac{c_b (U - U_i)}{T_w} \qquad (1.1a)$$

where:

F = the fraction of sea surface subject to breaking waves per unit time (sec^{-1})

T_w = the peak wave period (sec)

U = wind speed (m/sec)

U_i = wind speed at the initiation of breaking waves (5 m/sec)

c_b = constant (~ 0.032 sec/m)

This equation is widely used but does not account for wave induced turbulence except through the tumbling breaker mechanism. A graph of this function is shown in Figure 3, (labeled as Delvigne).

Delvigne suggest that non-breaking processes might also contribute to droplet formation, but the actual process is unknown. In a paper by Lehr and Simecek-Beatty (2000), the authors reviewed other studies that parameterize breaking wave area and suggested that Delvigne's value for U_i

is too high and does not properly simulate "non-breaking" turbulence sources. They also present several alternative formulations. When observing wave development at low wind speeds, the wave shape changes from nearly sinusoidal for winds less than about 2.5 m/s to trochoidal for winds greater then this threshold. It seems at least plausible that under trochoidal wave forms, the sharper crests and associated higher shear zones could introduce local pockets of turbulent mixing. With this in mind, equation (1.1a) was modified with the value of U_i = 2.5 m/s. This value is also shown in Figure 3, labeled as Galt (mod). This function does introduce mixing at lower wind speeds as intended, but also gives larger values over the entire wind range. There is no reason to expect that Delvigne's values for stronger wind speeds have systematic errors so a third version of the equation, (1.1b) labeled as "Corrected", is given where the c_b constant value is reduced by 19% to give consistent values at higher wind speeds. The formula given by this heuristic argument turns out to be nearly identical to one of the forms suggested by Lehr and Simecek-Beatty (2000).

$$F = \frac{0.027(U - 2.5)}{T_w} \qquad (1.1b)$$

A somewhat different approach was taken by Ding and Farmer (1994). In this work they describe a study where subsurface hydrophones were used to detect plunging breaker noise associated with bubble formation. This is more directly related to the mixing that would create oil droplets, but acoustic sensitivity issues make it difficult to detect low wind speed cases due to ambient noise levels. Thus their study does not directly shed any light on turbulence induced by trochoidal wave forms but it appears that

extrapolation of results could be used for these values. The formula presented in their work is as follows:

$$F = 0.00118\, U^{1.03} \qquad (1.1c)$$

This equation is also plotted in Figure 3 for comparison. Ding and Farmers approach for wind speeds below 4 m/sec is admittedly an extrapolation beyond the measurements, but subsequent numerical analysis suggests that the final model results are not particularly sensitive to which curve is followed. For this study the Ding and Farmer formulation was used with a lower limit of 3.0 m/s for the wind speed as a cut off.

Figure 3 -

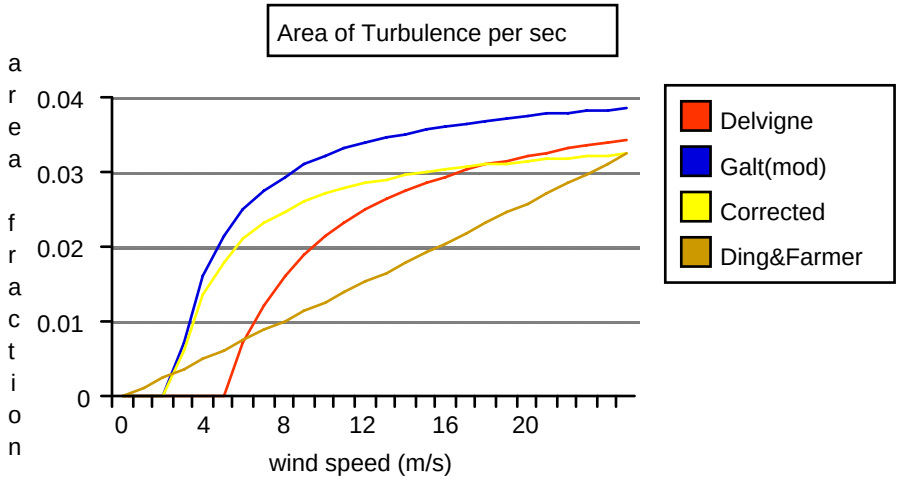

The next step in developing our simulation is to integrate the instantaneous fractional area of breaking waves given in equation (1.1c) to match the computational time step used in the ROC (nominally one hour). We start by assuming that we are in a slick. At a particular instant the fraction of the slick area subject to turbulent droplet formation is given by F_1 which is just a function of wind speed.

After an interval dt_F we can again obtain an estimate F_2 and calculate the additional fraction of the slick area that is subject to turbulent mixing and we expect:

$$A_1 = F_1; \qquad A_2 + (1.0 - A_1)F_2 \ldots\ldots \tag{1.2}$$

And this leads to the following differential equation:

$$\frac{dA}{dt} = (1.0 - A)F$$

Which can be easily integrated subject to $A(0) = 0$ and a computational time step of ΔT to give:

Fractional area where mixing takes place

$$A(\Delta T) = (1.0 - e^{(\frac{F\Delta T}{dt_F})}) \tag{1.3}$$

And the fractional area where mixing does not take place

$$A^*(\Delta T) = (1.0 - A(\Delta T)) \tag{1.4}$$

Although it is easy to hypothesize these equations there are several scaling issues hidden in the time constants dt_F and ΔT that need to be considered.

The first is how big does dt_F have to be so that the sequential estimates of F are not so dependent on each other as to invalidate the assumption given in equation (1.2). The dimensions of F given by Delvigne

are specified as (1/sec) but this is dictated by energy considerations and is used in Delvigne's equation 2 to predict an instantaneous rate of droplet formation. What we actually need is an integral of this instantaneous rate over some time increment and for this we must consider the actual persistence of areas of breaking waves. To get a better understanding of this we may consider the following experiment. At random time (t_1) under steady wind conditions *U* we take a vertical picture of the sea surface from a high mast mounted on an offshore platform and this image is analyzed by digitizing the fraction of area covered by breaking waves. We would expect the digitized fraction to be approximately the value *F*. If we were then to digitize a second picture that was taken one second after (t_1) and look at the correlation between "breaking" areas we would not expect them to be independent of each other. In fact if we were to do such an auto-correlation for a time series of pictures we would expect to come up with a figure similar to Figure 4. For short periods, areas of "breaking" would be well correlated, at longer lag or lead times they would essentially independent. This auto-correlation distribution defines a time period over which any particular *F* value would represent an independent estimate of the area covered by breaking waves, and equation (1.4) would be a fair representation of the process.

Figure 4-

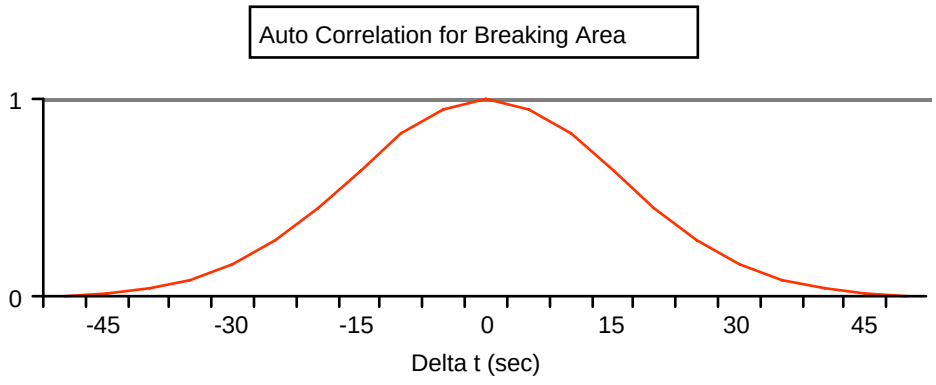

The correlation time scale is not the same as the breaking wave duration time scale defined by Ding and Farmer because their values look only at individual waves within a somewhat correlated wave field. Wave period is a natural time scale for the problem and it is tempting to associate the time scale dt_F with the wave period used in equation (1.1). Several numerical experiments using this approach did not lead to any believable results. It was concluded that since the wave spectrum is made up of a complex combination of periods, and the breaking process is quite nonlinear, this would not be a simple relationship. The next approach was to ask experienced observers what they thought the auto-correlation time scale would be, based on their intuition. This informal approach leads to estimates in the tens of seconds range. A numerical experiment using several different values for dt_F is shown in Figure 5. Obviously scaling on one second or wave period leads to complete mixing for all wind cases which does not seem realistic. And on the other extreme, scaling on 60 seconds gives slightly over 80% of the surface subject to breaking after an hour of 20 m/s winds. Having spent some time at sea under those conditions, this seems to me to fall somewhat short of the mark. In addition, studies by Melville (1994) estimate 90% if the total energy lost from a breaking wave field was dissipated within 4 wave periods. This suggests that an intermediate scaling of dt_F equal to 30 seconds would be a plausible starting value for this study.

Figure 5 -

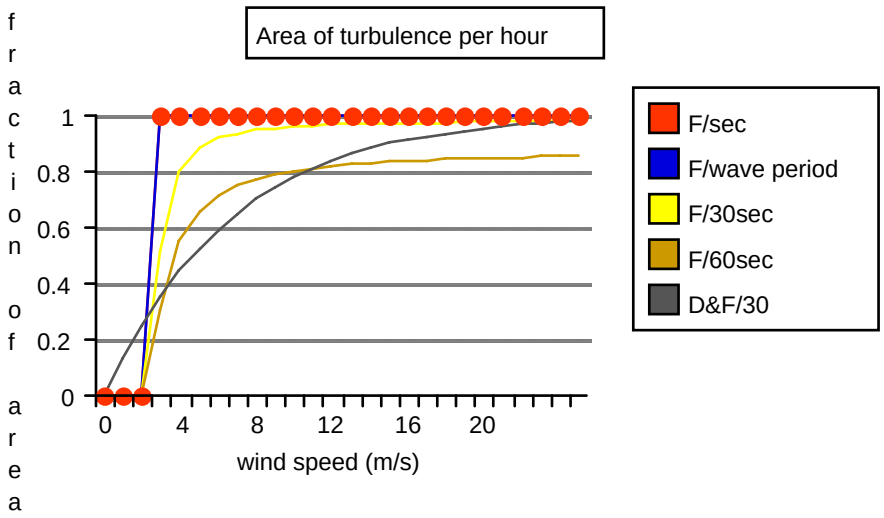

In Figure 5 the first two curves fall on top of each other and so the values are plotted as small dots.

The second time scaling issue with equations (1.3) and (1.4) is associated with the proposed ROC model's computational time step ΔT of one hour. There is an inherent assumption that oil droplets that are submerged will typically refloat and that this will result in their resurfacing. It is also assumed that this process will not be rapid enough for them to have a significant probability of being mixed again during the same time step. If this assumption is not valid, then it will be necessary to choose a different ΔT_d value such that:

$$\Delta T = n\Delta T_d \quad \text{where n is an integer} \qquad (1.5)$$

Then run the droplet sub-model as an n-step process within the larger computational time step of the model. With $dt_F = \Delta T_d$ and ΔT = 1 hour, n would be 120 which is easy enough to do computationally but it also implies some droplets may not be likely to resurface during the time step dt_F. This requires us to develop a "mix" and "remix" strategy that will be introduced later in this study.

Having defined the fractional area over which droplets are expected to form it is necessary to come up with an estimate of the depth to which this mixing will carry particles. Delvigne considers this issue and gives the intrusion depth as:

$$Z_i = 1.5 H_b \tag{1.6}$$

Where:

H_b = height of the breaking waves.

1.2 - Droplet Size Distribution;

The mass fraction distribution of oil droplets that are formed from a slick is given by Delvigne's equation 2 as:

$$Q(d) = C_0 D^{0.57} d^{0.7} \Delta d (S_{\text{cov}} F) \tag{1.7}$$

Where:

Q(d) = entrained mass rate of oil droplets with droplet size interval Δd centered on size *d*

C_0 = oil dependent constant

D= energy available from breaking waves

F = fraction on surface subject to breaking "energetic" waves

S_{cov} = fraction of the surface covered by the oil slick

Delvigne provides a separate equation for the wave energy. His equation (5) is:

$$D = 0.0034\ \rho_w g H_{rms}^2 \tag{1.8}$$

For this study we will only be applying this equation within a contiguous slick, so we will assume that S_{cov} = 1.0. In addition, under steady winds, the only time dependence in equation (1.7) is in the F term whose integration to fit the computational time step was the subject of the previous section. This was described in equation (1.3). Using these assumptions equation (1.7) in integrated form over the computational time interval is:

$$Q(d) = C_0 D^{0.57} d^{0.7} (\Delta d) A(\Delta T) \tag{1.9}$$

A plot of the general shape of this distribution is shown in Figure 6.

For each particular wind value, D is fixed and the mass fraction distribution of droplet sizes follows a $d^{0.7}$ power law. The total mass fraction of all the droplet size classes cannot exceed unity, so this integral constraint determines the largest droplets that will be formed for that wind energy. It can be seen from Figure 6 that high wind cases create smaller droplets as would be expected. For any particular wind speed and maximum droplet size and the total mass of the droplet classes is fixed. If this exceeds the mass of oil in the surface slick then all of the oil could end up as droplets in the water column.

Figure 6-

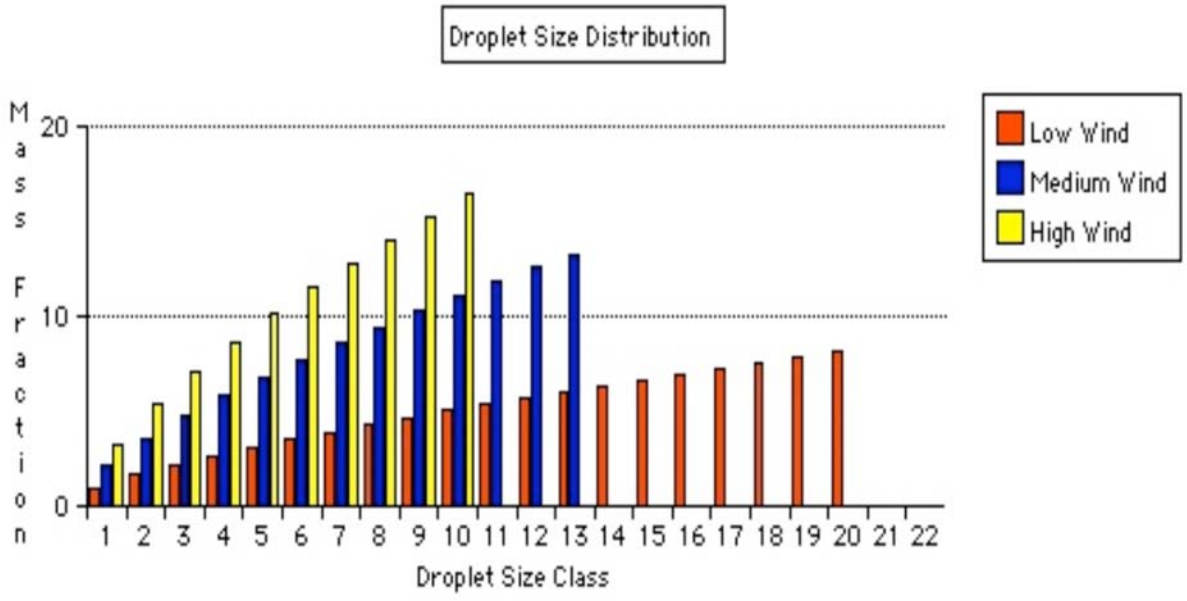

1.3 - Refloating of Droplets:

Oil droplets will remain buoyant when they are forced under water and re-float slowly to the surface. The speed with which they rise will depend on a number of factors. For droplet diameters less than 0.0002 meters the balance between their excess buoyancy and the frictional drag controls the rate of refloating. This balance is described by Stokes law, *Shepard (1963).*

$$w(d) = \frac{1}{18}\frac{(\rho - \rho_{oil})}{\rho \nu_{water}} g d^2 \qquad d < 0.0002\,(meters) \qquad (1.10)$$

where v_{water} is the kinematic viscosity of sea water and $(\rho_{oil} - \rho)$ is the difference in density between the oil droplet and sea water. For droplets that have a diameter greater than 0.01 meters, the force balance is between the buoyancy and the form drag created as the droplet develops differential pressure over its surface. In this case the controlling equation becomes:

$$w(d) = \sqrt{\frac{8}{3}(\rho - \rho_{oil})gd} \qquad d > 0.01(meters) \qquad (1.11)$$

Work by Ming and Garrett (1998) also present a good physical description of oil droplet behavior. Typically, studies that consider droplets using Delvigne's work are concerned with dispersion of oil and focus on droplet sizes that will rise so slowly that they are essentially removed from the surface slick. This would be droplets much less than a millimeter in diameter. Our interests are quite different. The focus on this study in on droplets that are only mixed below the surface for short periods ($\sim dt_F$) and are thus nominally considered as part of the surface signature of the oil. The submerged droplets are still part of the oil slick and just represent a fraction of the oil that moves more slowly in the downwind direction. This means that we will have to consider droplet diameters that fall between the two limiting classes expressed in equations 1.10 and 1.11. For these cases, Shepard suggests a smooth interpolation. Using this approach, Figure 7 shows the rise speeds for droplets in the 0-10 mm range for a number of different oil/water density differences.

Figure 7 -

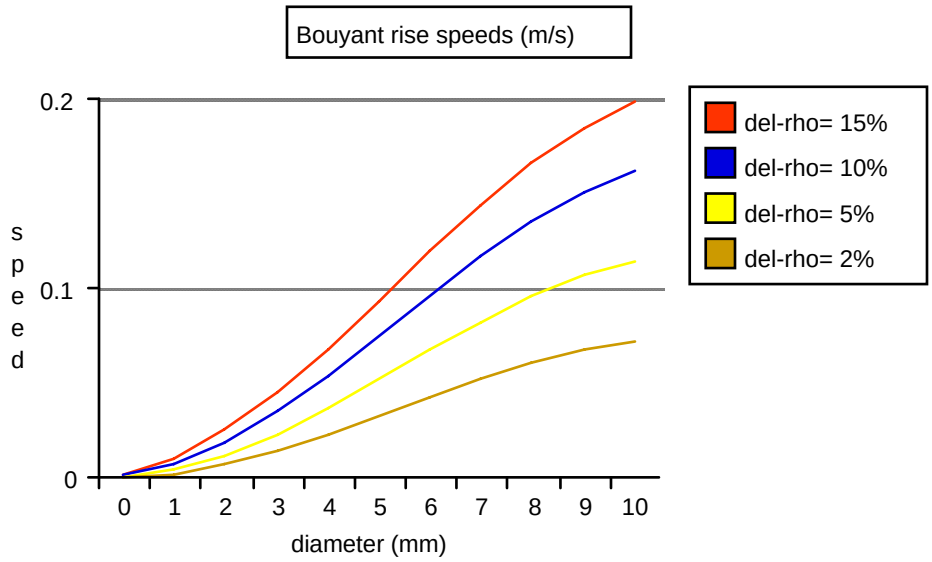

We do this by using a Hermite cubic that matches the value and first derivative of the Stoke's formulation on one end and the form drag equation on the other. This gives us a smooth and twice differentiable formulation over the gap, which exhibits the Stokes quadratic droplet dependence on the lower end of the curve and the form drag square root droplet dependence on the upper end of the range. The general equation for vertical droplet velocities is: (where the c_i for i=0..3 coefficients in the intermediate size range depend on density)

$$= \frac{1}{18}\frac{(\rho - \rho_{oil})}{\rho \nu_{water}} g d^2 \qquad d < 0.0002\,(meters)$$

$$w(d) \quad = c_3 d^3 + c_2 d^2 + c_1 d + c_0 \quad 0.0002 < d(meters) <= 0.01 \qquad (1.12)$$

$$= \sqrt{\frac{8}{3}(\rho - \rho_{oil})gd} \qquad d > 0.01(meters)$$

It should be noted that in Figure (7) droplet sizes range from zero to ten millimeters. The inclusion of large droplets reflects the focus of this study which is to consider droplets that do not naturally disperse, but rather rejoin the surface slick quickly.

Perhaps an easier way to think about this process is to consider the amount of time it takes for an oil droplet to resurface after turbulent processes have mixed it down below the surface.

Turbulent mixing process will tend to diffuse slowly moving droplets away from the surface and are ultimately responsible for "natural dispersion" of oil slicks, but for droplets in the one-millimeter and greater range this process is not effective. For all practical purposes, we can simply assume that droplets move back to the surface at their buoyant velocities. Taking this approach we note that different size waves will mix droplets to different depths, but for re-float time scaling purposes we can consider droplets resurfacing from a one meter depth. The results of these calculations for time in minutes are shown in Figure 8. These results span a wide range so the results are given on a log scale. It can be seen that very small droplets will take on the order of thousands of seconds (~hour) to resurface. On the other extreme, droplets that are at the high end of the range will resurface in half a minute or less. This is shown in Figure 8 as the 30s-cutoff. Given a particular wind mixing depth and buoyancy difference, droplets larger then this cutoff will essentially always be associated with the surface slick and not take part in the subsurface transport "slow down".

Figure 8-

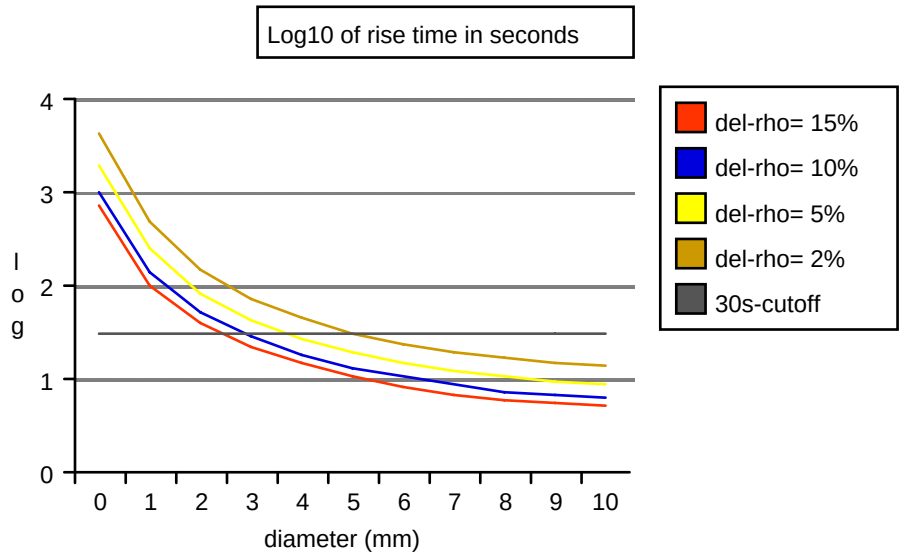

The droplet "rise time" introduces a third time scale into the problem. From Figure 8 we can see that the smallest droplets will refloat at time scales that approximate the one hour computational time step used within the ROC program while the larger droplets will resurface at time scales that are comparable to or less than the "surface wave auto correlation time" suggested in Figure 5. This is a pretty clear indication that our algorithms should consider a "two stepping" process where a shorter time step computational loop is imbedded in the longer time step algorithm. To close in on how to do this we need to put some actual numbers into the Delvigue algorithms and see what they suggest.

1.4 Droplet Mix and Remix Process:

Using Delvigne's formulation we expect that each energetic event will mix some fraction of the surface slick into various droplet classes in the wave mixed zone. We now need to consider the statistical pathway of these various mass fractions. At each time step, some fraction of the surface slick

is partitioned into droplets and mixed into a shallow sub-surface layer. At the same time some portion of droplets (depending on *A(U)*) already mixed into that layer are remixed and added to the new droplets. Also some of the droplets from previous mixing (dependent on *1-A(U)*) are not remixed and simple move back towards the surface at the flotation speed *w(d)*. For any particular droplet size class we can represent the process results with the following figure:

Figure 9 - (for each droplet class)

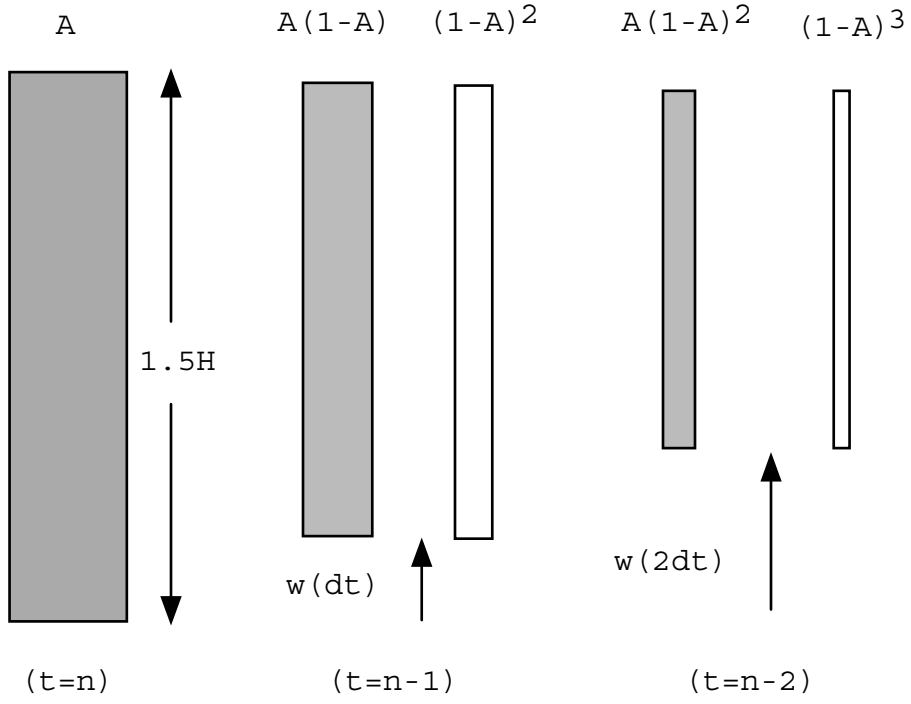

At the beginning of time step *n*, the freshly mixed droplet mass for a droplet class will be fraction *A* from the surface slick, plus fraction *A* of the *(1-A)* fraction which were not mixed during the previous mixing event, leaving fraction $(1-A)^2$ unmixed, etc. From this we see that each unmixed fraction of each energetic event is moving back towards the surface while each new event mixes droplets from the surface and remixes a fraction of all the

previous mixes. The total representation of mixed and remixed droplets at each time step will be the shaded portion in Figure 9.

An algorithm representing this process could be written in a recursive form. A simpler approach is to aggregate all the remaining oil droplets for each size class at the end of each time step, being careful to conserve both mass and the mass weighted vertical position of the residual. This limits the computation to a single mix/remix for each time step and each droplet size class, without introducing any significant errors.

1.5 Droplet Horizontal Movement

Below the free surface there will be a boundary layer current that can be considered as a constant stress region (Prandtl's layer) associated with the finite amplitude surface waves. For this simulation we will assume a logarithmic depth dependence with surface velocities of 3 percent of the wind speed, as described in Kinsman (1965) or the ADIOS manual. A typical curve is shown in Figure 10.

Figure 10 -

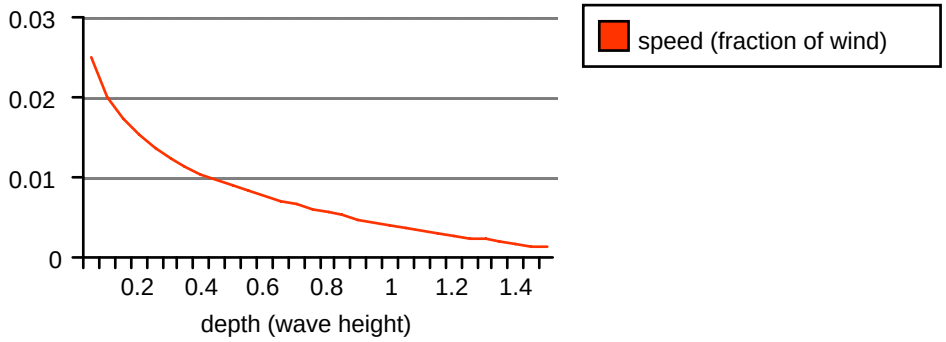

Using the droplet size class depths obtained during the mix/remix calculations we can enter the curve representing the horizontal speed shown in Figure 10 and calculate the downwind transport of each of the droplet size classes relative to the surface drift (which will also be the drift of the unmixed fraction of the slick). The smaller droplets will be seen to lag behind the larger droplets and surface portion of the slick. For each new dt_F time step, a new mixing of the surface slick will take place. The mass fraction of new droplets created will be added to the droplets left over from the previous step and remixed. As the model progresses, this sorting process leaves a heavier mass fraction of the slick moving to the downwind position in the slick.

We can note that the portion of the slick that remains consistently on the surface will move at about 3% of the wind speed, while the smaller droplets that spend a significant fraction of their time mixed throughout the wave mixing zone will have an average downwind drift of about 0.5% of the wind speed. This clearly contributes to the anisotropic spreading of oil slicks under the effects of a surface wind.

1.6 - Numerical examples

To carry out some numerical explorations of these component algorithms we need to consider how to handle the various terms that are parameterized in terms of various wave heights. Obviously waves and their statistics come in many different forms. Considering the nature of our proposed simulation, we will consider the wave to be a fully developed equilibrium spectra; i.e. not limited by fetch (typical of inland waters) or duration (typical of squall line weather patterns). The relationship between

wind speed and various wave parameters is given by H.O. Pub. No.604. For this study, a fully developed Pierson-Moskowitz spectra is assumed. This leads to the following equation for an energy parameter and average period as a function of wind speed. (After converting speed to m/sec)

$$E_{(m\,2)} =< \varsigma^2 >= (3.1614\,e-5)U^4_{m/\sec} \qquad (1.13a)$$

$$T_{peak\,(hertz)} = 0.750\,U_{m/\sec} \qquad (1.13b)$$

Then we expect the following relationships between the energy and various spectra wave height parameters:

a) Significant wave height:

$$H_{1/3} = 0.02244\ U^2_{m/\sec} \qquad (1.14)$$

b) Average wave height:

$$H_{average} = 0.0140\,U^2_{m/\sec} \qquad (1.15)$$

c) Typical breaking wave height:

$$H_{breaking} = 0.02854\ U^2_{m/\sec} \qquad (1.16)$$

These relationships provide all of the required wave information used in Delvigne's formulation in terms of the wind speed in meters per second measured at a standard 10 meters height. Estimated wave values are shown in the following figure.

Figure 11 -

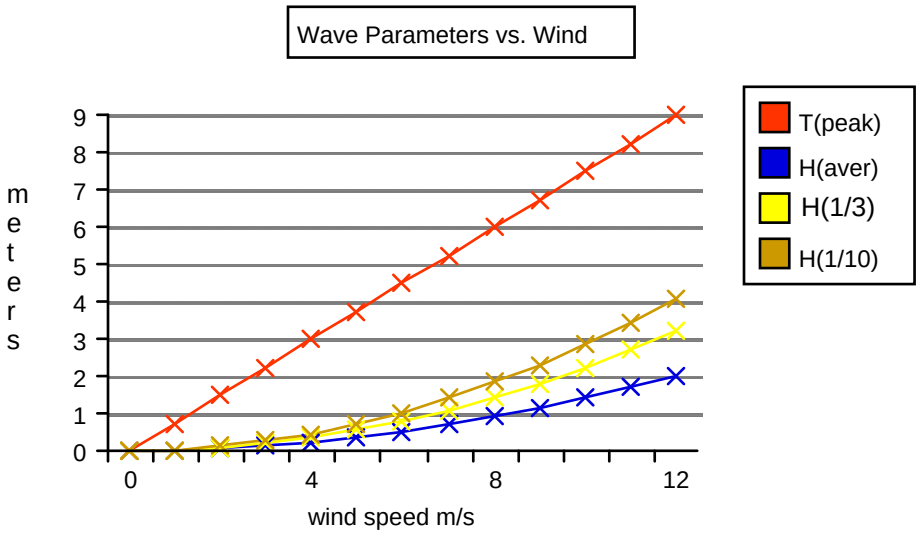

In Delvigne's equation (1.7) there is an energy term related to the breaking waves. This term is given in Delvigne (1.8) and with the wave spectra data this can also be described in terms of the wind speed as follows:

Figure 12 -

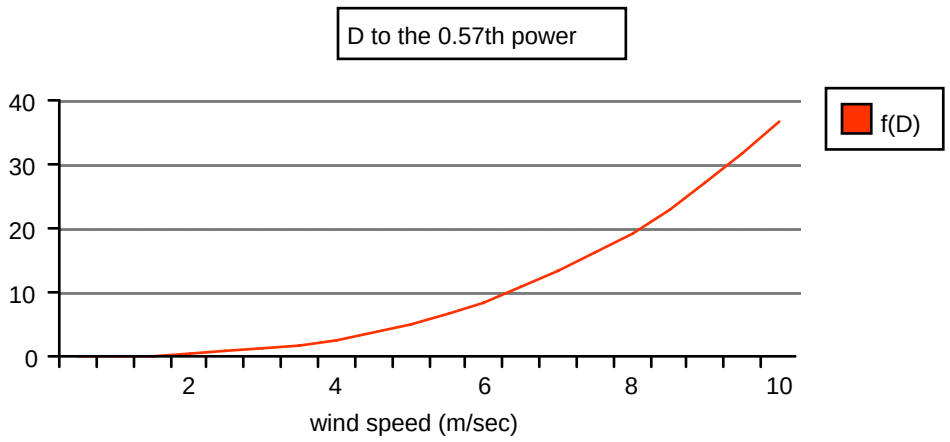

Finally Delvigne's equation (1.7) uses a constant C_0 that describes the ease with which a surface slick will break into droplets. Delvigne examined only a limited range of oils of relatively low viscosity. Dr. Mark Reed at Sintef has expressed some interest in this problem and is looking into research to extend Delvigne's work for higher viscosity oils (viscosity > 1000 cSt) (Personal communication). When this work becomes available, the data will certainly be of interest to this project. Delvigne suggests that his term may be proportional to the viscosity to the minus one power and used a value of (C_0= 840) for relatively fresh North Slope Crude. In another study associated with the development of NOAA's oil weathering model ADIOS, Roy Overstreet came up with the formula:

$$C_0(\nu_{oil}) = 2400 \exp(-73.682\sqrt{\nu_{oil}}) \qquad (1.17)$$

Where the (ν_{oil}) term is expressed in kinematic units in the mks system. To convert from centistokes to mks:

$$\nu(mks) = 10^{-6}\,\nu(centistokes\ )$$

This gives the following relationship between C_0 and the viscosity of the oil:

Figure 13 -

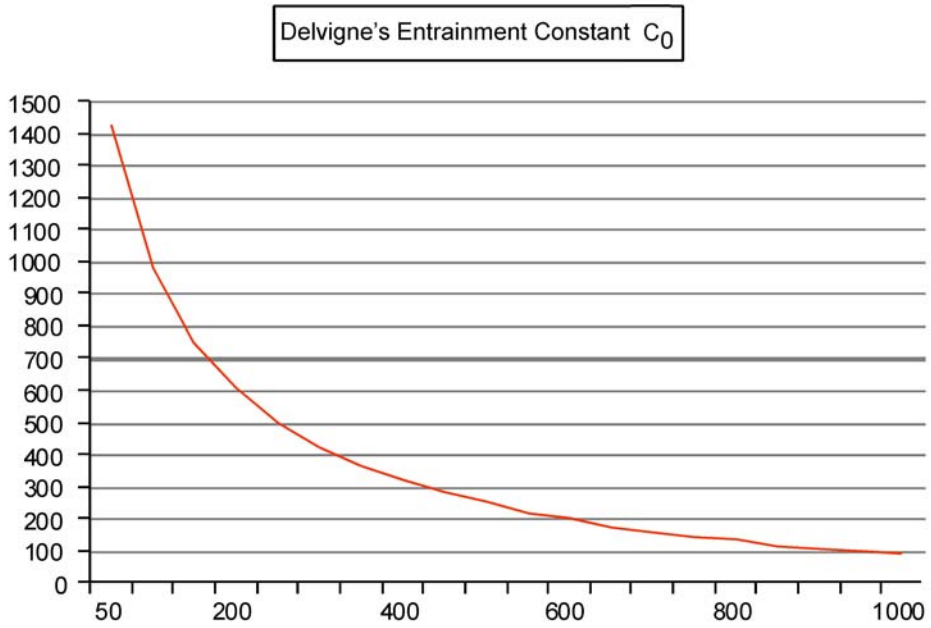

As the oil becomes increasingly viscous, this coefficient will become small and eventually wave action will be unable to tear the surface slick into small droplets. In effect this process will turn itself off, as field observations suggest.

1.7 Droplet Algorithm:

Having described all of the physical processes that are relevant to the droplet model, we now can outline the general algorithmic procedure used in the model. Consider the following steps:

a) We start by considering a particular environmental setting with the wind speed *U (m/sec*) given. With this value we can calculate the depth of the wave mixing zone (Z_b) which will be 1.5 times the depth of the breaking waves as given by equation (1.16) in terms of the wind speed.

b) With the depth (Z_b) and the time step used in the mix/remix section of the model (30 sec), we can calculate the vertical rise rate of a droplet that would regain the surface before the end of the time step $V_{cutoff} = Z_{b/30.}$

c) Given V_{cutoff} we can solve the inverse of equation (1.12) to obtain the droplet cutoff value D_{cutoff}. This droplet size depends on the wind speed and the density of the oil/mousse, which of course could vary with time and weathering state during a spill. This droplet size cutoff has an important physical meaning in the model and turns out to be an important parameter. Droplets that are larger than the cutoff value will never remain submerged long enough to be significantly slowed down, and will tend to move downwind at the 3% of the wind speed associated with the surface drift. On the other hand, droplets smaller then this cutoff will be below the surface for larger fractions of the time and will be subjected to the reduced speeds in the logarithmic current profile below the surface. When they ultimately return to the surface, they will lag behind the larger droplets that remained on the surface.

d) Given the D_{cutoff} as the upper limit of droplets that we need to consider, we define 20 droplet size classes that span the range $0 < d < D_{cutoff}$ which will be used as the basic discrete elements in the Delvigne formulation and the mix/remix stepping algorithm.

e) Now with the addition of the oil/mouse viscosity, we have everything we need to calculate the droplet mass distribution using Delvigne's equation (1.9). The twenty droplet classes cover the range of droplet sizes that will be moving up and down within the wave mixed layer and contribute to the differential downwind drift. It is important to note that this distribution will be characteristic of a particular set of environmental conditions (wind speed and water temperature) and oil weathering state (density and viscosity). The results can be best understood in the following model schematic:

Figure 14 -

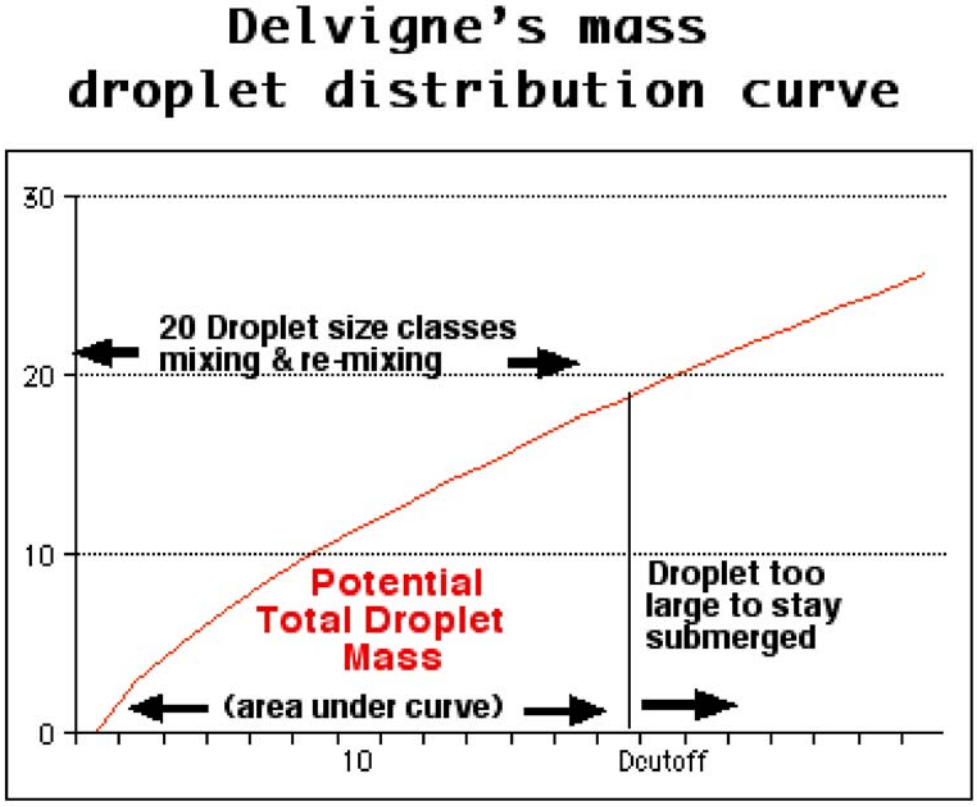

This sketch is fundamental in understanding the workings of the droplet model. Droplets that are larger than the D_{cutoff} size may be formed but they will resurface so quickly that their mass will not contribute to the differential drift within the slick. This critical cutoff is a function of the wind speed and the buoyancy of the oil. The curve in red is calculated from Delvigne's formula which in turn depends on the wind speed and the viscosity of the oil. The area under the curve represents the maximum potential mass of submerged droplets that could be moving below the surface and contributing to differential drift of the slick. The quantity (DropletMass) will have units of mass/area and plays a critical role in scaling the model.

From a general understanding of the Delvigne formulation we know that if the mass of the surface slick's mass/area is less than DropletMass then an energetic mixing event will completely drive the slick to the droplet distribution and any excess droplet capacity out of the total potential will be unfilled. This condition will occur when the non-dimensional ratio of SlickMass/DropletMass is < unity. An alternate case will occur when the surface slick's mass/area is greater than DropletMass. In this case an energetic event will completely fill the potential DropletMass and the excess will remain on the surface moving downwind at the maximum surface speed. This condition will occur when the non-dimensional ratio SlickMass/DropletMass is > unity. From this argument we can expect that the scaling of the droplet model will depend on the ratio SlickMass/DropletMass. This is the case and we will refer to this ratio as the model scale, or scale factor.

f) With the above settings the algorithm now simply goes through stepping of the mixing and remixing for each of the droplet classes calculating the mass and vertical positions for each class as it is formed and the same for the residual droplets from previous mixing events. These fractions of the mass are then advected downwind based on their vertical position in the surface shear layer. The distribution stabilizes quickly and when downwind distance is scaled against the surface drift no change is seen after 120 steps, or a one hour run time.

1.8 Droplet Model Results:

Model results can be summarized easily when plotted in terms of the droplet scale factor. The raw data from the model is in terms of speed downwind vs. cumulative slick mass. In this figure, all of the speed values have been scaled to the surface drift, which is 3% of the wind speed. In all

the cases with the scale value clearly above unity, there is some portion of the slick that shows no significant reduction in speed and moves downwind at the maximum rate. As the scale factor is reduced, a larger and larger fraction of the total oil starts to lag behind the faster surface portion. As the scale factor approaches unity and falls below it, the curves show that virtually all of the slicks mass shows some reduction in speed compared to the maximum surface value. The energetic mixing events therefore include all of the surface slick in the droplet activity and all the oil is slowed down to some extent.

Figure 15 -

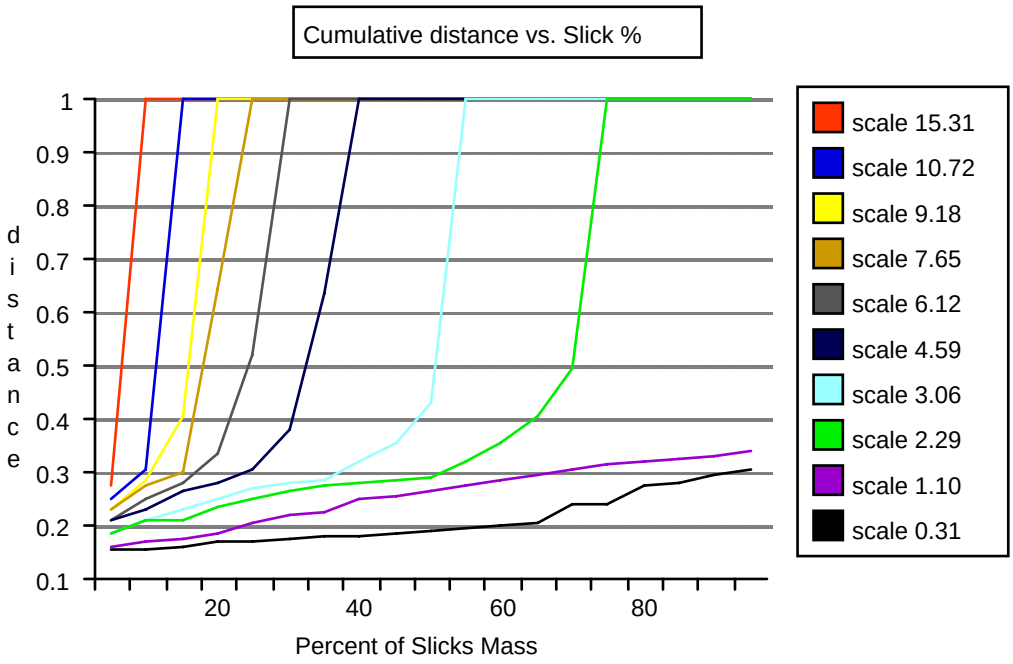

The amount of oil in each downwind segment of the slick will be related to the bunching, or clustering of shown in Figure 15. A measure of this will be the inverse of the derivative of the curve itself. This would be a measure of the oil mass per relative distance downwind throughout the slick. This is equivalent to a raw estimate of the oil mass in droplet mass per distance downwind. The actual appearance of oil thickness is a little more complicated than simply whether or not it is in the water column, and this can be seen by a little dimensional analysis. The downwind spreading of the droplets has been carried out as a one-dimensional model. As a droplet or mass of droplets appears at the surface, the rising column will have to spread out radially in two dimensions. In addition, the speed at which the column of droplets is supplying oil to the surface will depend on the buoyant velocity of the droplets themselves. From these considerations, it seems likely that a useful measure of relative thickness could be estimated by taking the square root of the inverse derivative from Figure 15 and

multiplying by the vertical droplet speeds. Applying this to a set of scaled cases results in the following set of thickness estimate curves:

Figure 16 -

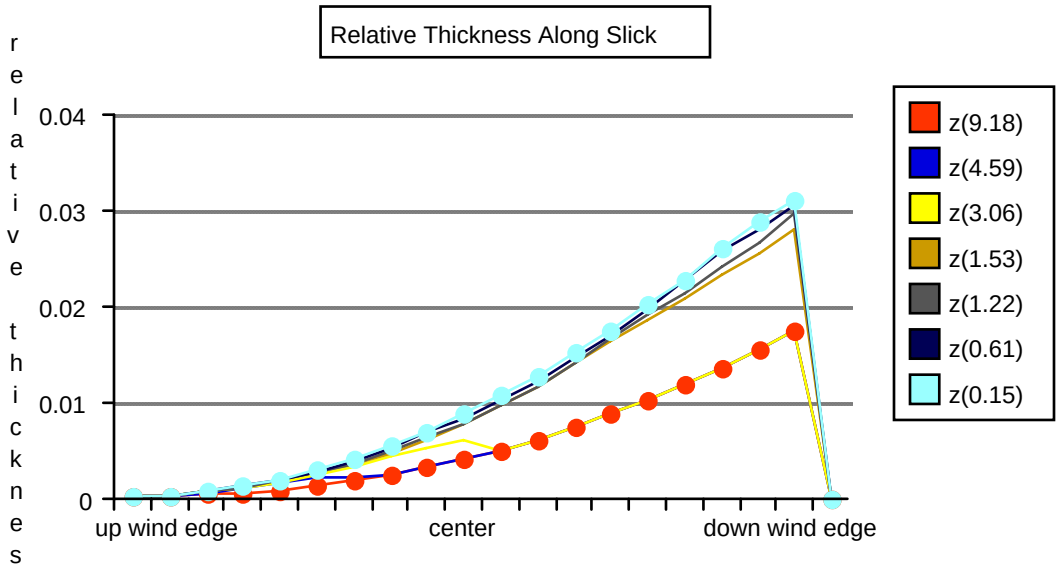

In this figure we included scale values that ranged from well above to well below unity. The values associated with high scale values (represented by the red dots) tend to fall nearly on top of each other. Likewise values associated with small scale values also tend to bunch (represented by the light blue dots). In all cases there is a clear tendency for the spill thickness to increase in the downwind direction, leading to the "comet shape" suggested in the beginning of this section.

The final objective of the droplet model was to provide an estimate of the ratio of the maximum thickness of a contiguous slick to the mean thickness that would be calculated from a simple mass-balance oil weathering model. From the data presented in Figure 16 we can obtain a relative mean thickness and a relative maximum thickness. The ratio C1 is defined as a function of wind speed, oil density, oil viscosity and average

slick mass or thickness. As we have seen, however, all of this variability is included in the droplet model scale factor. With this in mind we set the model up to run using physically realistic but random distributions of all of the above parameters and present the results in terms of C1 vs. scale factor.

Figure 17 -

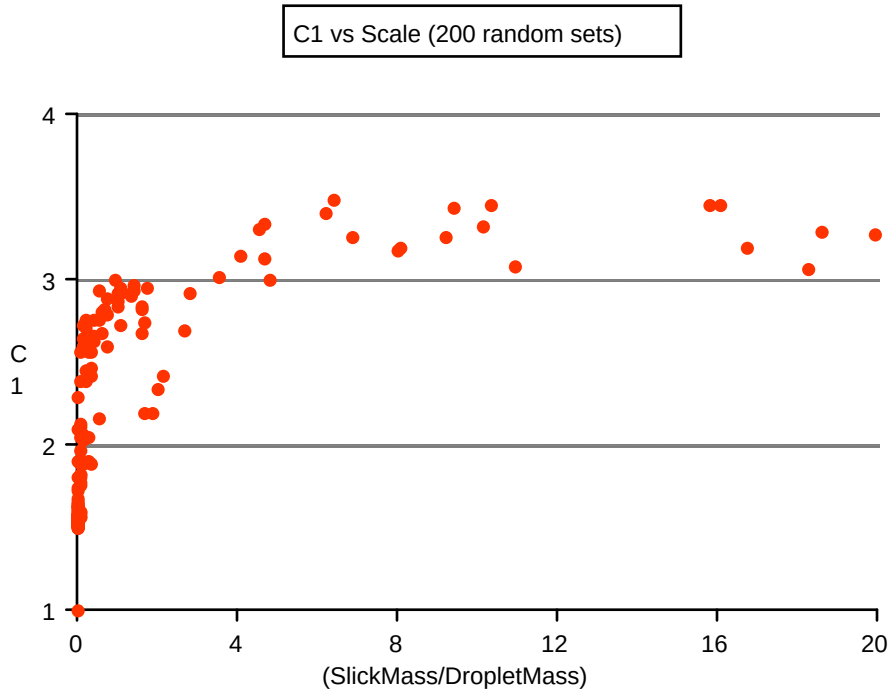

This figure clearly shows the influence of the scaling factor on the oil thickness maximum's relative to the mean thickness over the area of the slick (C1). For values of the scale greater than about six, the continual mixing and remixing process works on only a fraction of the total slick and an equilibrium is established. C1 levels off to a more or less constant level at about 3.2. High scale values correspond to (thick) heavy surface slicks (relative to the DropletMass). Early in the spill this would be common behavior because of the thickness.

Higher scale values would also occur if the DropletMass were to become small. This would happen if the density of the oil were very low (droplets would rise quickly) as would be expected initially for high API density oils while they remain thick slicks. Very viscous oils would also lead to small DropletMass and higher scale values. This might be expected as a trend when oil weathers and/or forms a mousse. The third factor that would lead to small DropletMass would be low wind speeds because the mixing depth would tend to be small. In the extreme case where there was no wind induced energetic events, the DropletMass would go to zero and a singularity would occur in the scale factor. The droplet model traps for this case and if the wind is below the 3.0m/sec threshold, it sets C1 to the correct default (unity) and does not run the mix/remix procedure.

The general trend in C1 as the scale factor becomes unity and below is to fall off and go through intermediate values on its way to the default of unity as scale values approach zero. We can also clearly see that there is more variability in the predicted values of C1 in this range. The simple scaling seems to be breaking down a little in this range. A consideration of the components making up the scale factor suggests why. If the scale factor is low it is either because the surface slick has become very light (thin) or the DropletMass has become very large. A large DropletMass could be caused by: a) very heavy oil (densities approaching neutral or even sinking). b) very low viscosity (high entrainment coefficient C_0 in Delvigne's equation) as might occur in refined products, and c) strong winds which would give a large wave-mixed layer depth. In all of these situations, the common factor is that the surface slick goes away. We would no longer be tracking a contiguous surface slick. Under these conditions a typical over-flight would report scattered sheen.

If the dropping scale values were due to oil density, viscosity, or spreading, the trend would likely be permanent. If it was due to high wind,

the scale values could go up again if the wind dies off. The slick would reappear as is commonly observed on actual spills.

References:

Delvigne, Gerard A. L. (1993) *Natural Dispersion of Oil by Different Sources of Turbulence*. IOSC pp. 415-419.

Ding, Li and David M. Farmer(1994) Observations of Breaking Surface Wave Statistics. JPO(24) pp1368-1387

H.O. Pub. No. 604 (1967) Practical Methods for Observing and Forecasting Ocean Waves. U.S. Naval Oceanographic Office.

Kinsman, Blair(1965) Wind Waves Prentice-Hall Englewood Cliffs, NJ. pp676.

Lehr, William J. and Debra Simecek-Beatty (2000) *The Relation of Langmuir Circulation Processes to Standard Oil Spill Spreading, Dispersion, and Transport Algorithms*. Spill Science and Technology Bulletin Vol. 6, No, 3/4 pp 247-253

Ming,Li and Chris Garrett(1998) The Relationship Between Oil Droplet Size and Upper Ocean Turbulence, Marine Pollution Bulletin Vol. 36, No. 12 pp 961-970

Moskowitz L.(1964) Estimates of the power spectrums for fully developed seas for wind speeds of 20 to 40 knots, Journal of Geophysical Research, Vol. 69 (24), p.5161–5179.

Shepard, Francis (1963) Submarine Geology 2nd Edition Harper and Row, New York, NY pp557.

Section Two: Langmuir Circulation

The following section is divided into three parts. First, schematic diagrams and observational results are presented to give users a better understanding of the general features of Langmuir circulation. Next, an operational model for Langmuir circulation is described. Finally, model results are presented and discussed.

2.1 General Description of Langmuir Circulation:

Langmuir circulation is a dynamic instability in the mixed layers of lakes, oceans, and other water bodies that are large enough to maintain a nonlinear interaction between Stokes drift and surface wind stress. Stokes drift is a rectified current generated by ordinary gravity waves. This interaction causes vertical vorticity to be transformed into downwind vorticity, producing a series of counter-rotating helices aligned with the wind (Craik and Leibovich, 1977). Langmuir circulation is commonly seen as surface "windrows", where lines of foam and bubbles from breaking waves, marine organisms, oil, and other flotsam are swept into narrow zones of jet-like motion, both downwind and vertically. Langmuir circulation is now believed to be a major contributor to the formation and maintenance of the mixed layer. The vertical motions are often strong enough to submerge normally buoyant material, such as oil.

For instance, Figure 1 is an aerial photo of oil on the water. The lower portion of the photo clearly shows the downwind beginning of Langmuir circulation.

Figure 1-

From NOAA, Hazardous Materials Response Division

A general picture of Langmuir circulation is shown in Figure 2.

Figure 2-

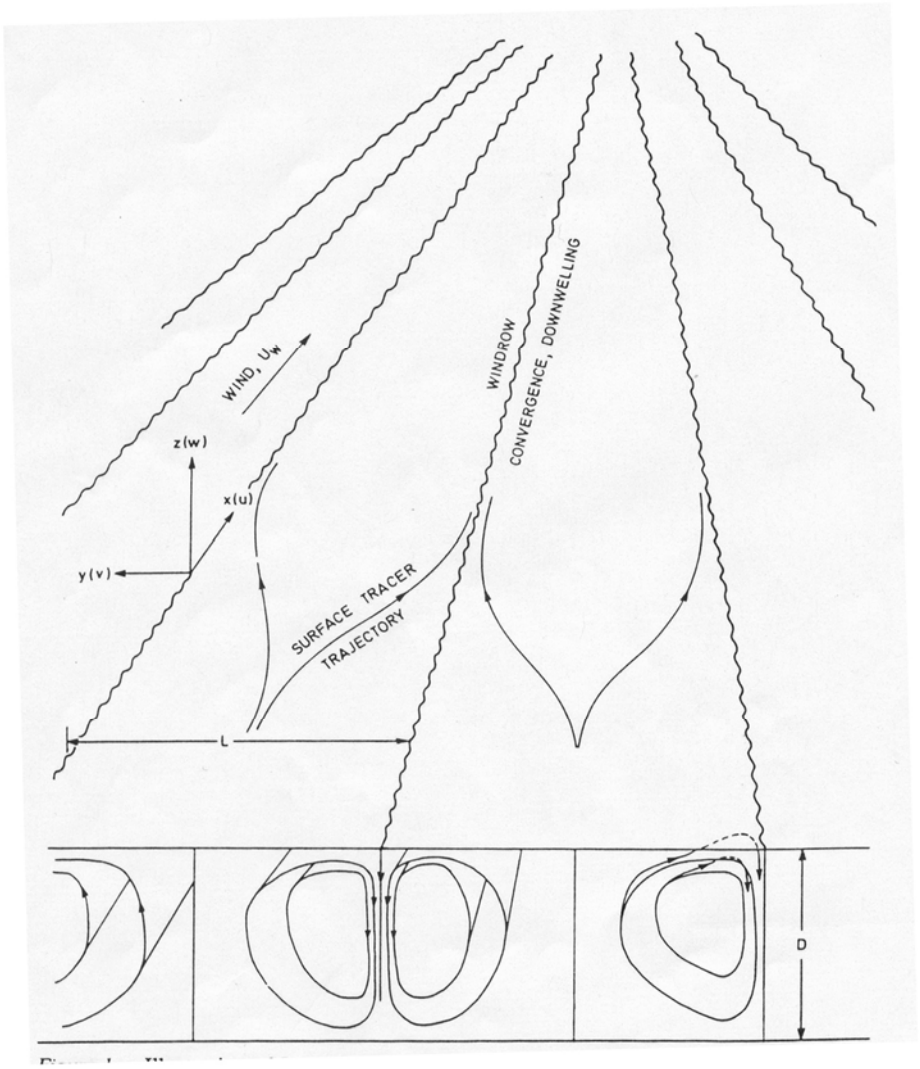

From Leibovich (1983)

Figure 3 shows easily-seen windrows of bubbles on Rodeo Lagoon, a shallow barrier island lagoon in Marin County, California. Careful examination of the photo also shows wave crests that are essentially perpendicular to the windrows.

Figure 3-

From Szeri (1996)

Although the windrows shown in Figure 3 are striking, they do not provide information about subsurface motion. Figure 4 helps fill this gap. Weller and Price (1988) made three-dimensional current profiles in the mixed layer, using vector-averaging current meters. The most striking features of these results are the strong downwind jets coinciding with the windrows, and the *equally strong* vertical jets below the convergences.

Figure 4-

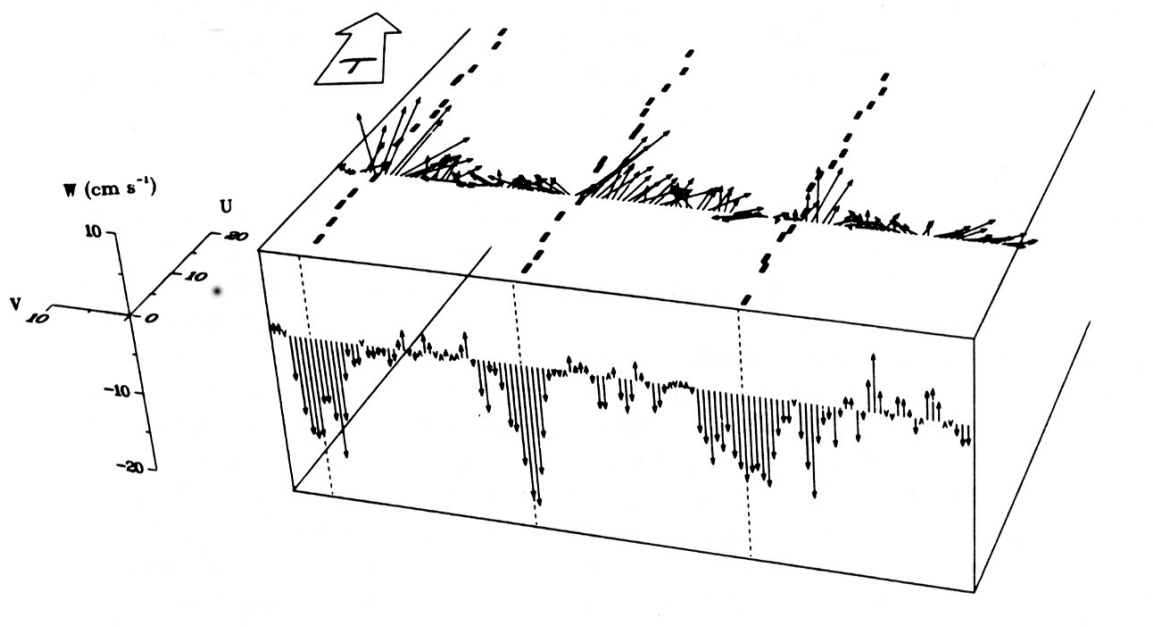

From Weller and Price (1988)

Thorpe (2004), Farmer and Zedel (1991) and others, using a variety of instruments, found similar motions. For instance, acoustic scattering methods have been an effective tool for detection of Langmuir circulation by measuring the spatial distribution of bubbles generated from breaking waves. These instruments are both bottom-mounted looking upward, and drifting looking downward (Thorpe, 2004). For instance, Zedel and Farmer (1991) used acoustic transducers suspended in the mixed layer below a freely drifting buoy. The instrument was equipped with simultaneous upward looking vertical sonars and horizontally directed side scan sonars, which produced three-dimensional bubble plumes characteristic of Langmuir circulation.

Figure 5) shows periodic bands of bubbles detected by side scan and upward looking sonar tethered to a freely, drifting buoy. Again, the results show the presence of Langmuir circulation.

Figure 5-

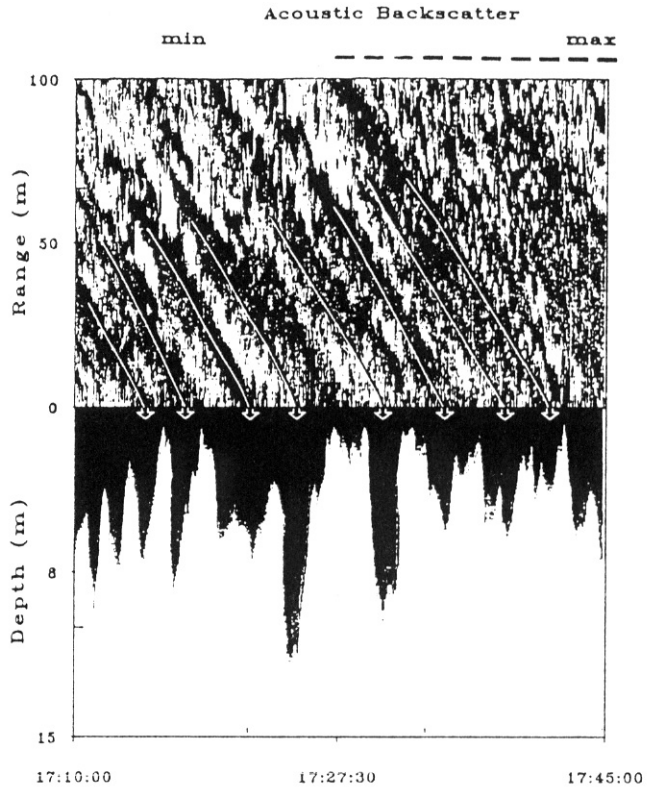

From Zedel and Farmer (1991)

Figure 6 shows an aerial infrared image of the sea surface of Tampa Bay. Downwind temperature streaks indicate the presence of Langmuir circulation. Note the remarkable difference in cell structure between the upper and lower halves of the photo. The reason for this difference is the presence of a weak temperature front that abruptly changed the cell spacing from wide to narrow.

Figure 6-

From Marmorino (2005)

2.2 – Langmuir Circulation Model:

The following discussion describes an operational computer model that can be used by spill responders to help assess the role of windrows as collectors of oil. Leibovich (1997) describes the formulation of the complete model for Langmuir circulation. The model is very complex and can only be solved numerically, which precludes its use in an operational mode. However, numerical explorations have been very useful in guiding the construction of a few simpler, operational models.

Leibovich (1997), under a long-term contract with the Minerals Management Service of the US Department of The Interior, developed a numerical spectral model that solves the equations governing the downwind Stokes drift velocity and the crosswind stream function representing Langmuir

circulation. The numerical model uses Fourier series in the spanwise direction, and Chebyshev polynomial expansions of vertically generated synthetic data for different combinations of key parameters. This was then used to make a much simpler, operational model to evaluate different spill scenarios.

The use of Fourier series and Chebyshev polynomial expansions allowed the numerical and operational models to be characterized by only two dimensionless numbers: the Rayleigh number, Ra, the ratio of wind and wave forcing to viscous resistance to Langmuir circulation, and the peak of the wave number spectrum, κ_p. Basically, the models depend only on wind, waves and mixed-layer depth. The simpler model, known as OILTRACK, makes best fits of the numerical results for distribution of the downwind velocities, lateral motions that sweep surface water into windrows, and downwelling at convergences, i.e., the Langmuir streamfunction. Input data consists of wind speed and direction; externally provided currents; mixed-layer depth; water temperature and salinity; and oil density and surface tension.

The Leibovich model has two very attractive features. First, it is based on fitted correlations to direct numerical solutions to the velocity and streamfunction equations and yet is simple enough to be implemented in MATLAB®. The equally attractive feature is the fact that the numerical model used 23 pairs of Ra and κ_p in order to *generate a synthetic data base* for OILTRACK's correlation algorithms.

The standard formula for surface wind stress, characterized by the so-called friction velocity is given by:

$$u_* = \left(\frac{\tau_w}{\rho_w}\right)^{\frac{1}{2}} = \left(C_D \frac{\rho_a}{\rho_w}\right)^{\frac{1}{2}} U_{10} \qquad (2.1)$$

This is the standard formula for wind stress (friction velocity), where ρ_a and ρ_w are air and water density respectively, C_D is the drag coefficient, and U_{10} is the ten-meter wind speed. For back-of-the-envelope scaling purposes $u_* \approx 0.001 \cdot U_{10}$ is generally adequate. For a more accurate estimate, the following correlations can be used (Large and Pond, 1981):

$$\frac{\rho_a}{\rho_w} \approx 1.2 \times 10^{-3} \qquad (2.2)$$

$$\begin{aligned} C_D &= 1.2 \times 10^{-3}, \text{ for } U_{10} < 11\text{m/s} \\ &= (0.49 + 0.065 U_{10}) \times 10^{-3}, \text{ for } 11\text{m/s} < U_{10} < 25\text{m/s} \\ &= 2.1 \times 10^{-3} U_{10}, \text{ for } U_{10} > 25\text{m/s} \end{aligned}$$

The Stokes drift is

$$u_s(z) = u_s(0) \exp(2\kappa_p z), \qquad (2.3)$$

where

$$\kappa_p = \frac{0.774g}{U_{10}} \qquad (2.4)$$

is the spectral peak of fully-developed waves in the commonly used Pierson-Moskowitz wave spectrum.

The surface Stokes drift for fully-developed seas is:

$$u_s(0) = 0.013 U_{10} \qquad (2.5)$$

The mixed layer depth is either prescribed (preferably) or is approximated to be twice the Ekman depth,

$$d_{mix} = 2d_E = 2\left(\frac{v_T}{f/2}\right)^{1/2} \qquad (2.6)$$

Where $f = 1.4544 \times 10^{-4} \sin(\text{latitude})$ is the Coriolis parameter.

The eddy viscosity coefficient υ_T lurks in much of the Langmuir circulation parameterization. Leibovich (1997) discusses the preference of obtaining the eddy coefficient as a result of large eddy simulation (LES) models rather than specifying it *a priori*. For instance, Skyllingstad and Denbo (1995) compute a bulk eddy viscosity by taking the ratio of the computed Reynolds stress and the mean velocity gradient. Leibovich (1997) expresses this result as $\upsilon_T \approx 0.06 u_* d_{mix}$, which is the choice used here.

The windrow separation L_s is either prescribed (for example, as observed from over-flights) or taken to be three times the mixed-layer depth (Smith and Pinkel (1986), Leibovich and Paolucci (1979))

$$L_s = 3 \times d_{mix} \qquad (2.7)$$

A sweeping time t_{sweep} is defined to be the characteristic time taken to carry oil the width of one dominant Langmuir cell and into the next convergence.

$$t_{sweep} = 86 \frac{d_{mix}}{U_{10}} \frac{\sqrt{g d_{mix}}}{U_{10}} \qquad (2.8)$$

OILTRACK computes the depth-dependent vertical velocity beneath windrows by a polynomial fit of the numerical simulations.

$$W(z) = -5.4\frac{u_*}{R_*}\sqrt{\frac{Ra - Ra_c(k)}{Ra_c(k)}}\tilde{z}\left(p_1\tilde{z}^2 + p_2\tilde{z} + p_3\right), \qquad (2.9)$$

where $\tilde{z} = z/d_{mix}$, the depth normalized with respect to the mixing depth. The constants (p_1, p_1, p_3) are given by

$$p_1 = \frac{2\tilde{z}_m + 1}{\tilde{z}_m{}^2(1+\tilde{z}_m)^2},\ p_2 = \frac{3\tilde{z}_m{}^2 - 1}{\tilde{z}_m{}^2(1+\tilde{z}_m)^2},\ p_2 = \frac{3\tilde{z}_m + 2}{\tilde{z}_m(1+\tilde{z}_m)^2}\ ,$$

where $z = \tilde{z}_m$ is the dimensionless depth of the maximum vertical speed. The numerical solutions give the following expression for $\tilde{z}_m$

$$\tilde{z}_m \approx -0.5 + 0.1318\frac{\kappa^2}{\left(1+1.0187\kappa^2\right)}.$$

The term R_* is the Reynolds number

$$R_* = \frac{u_* d_{mix}}{\upsilon_T} = \frac{u_* d_{mix}}{0.055 u_* d_{mix}} = 18.2 \qquad (2.10)$$

Finally, the term $r = \sqrt{\frac{Ra - Ra_c(\kappa)}{Ra_c(\kappa)}}$ involving the Rayleigh number and the critical value required for Langmuir circulation are, respectively,

$$Ra = 23.6\kappa R_* \qquad (2.11)$$

and

$$Ra_c = \frac{64\kappa^5}{1 - \kappa + \frac{\kappa^3}{3} - e^{-2\kappa}\left(1 + \kappa - \frac{\kappa^3}{3}\right)}. \qquad (2.12)$$

Figure 7 shows downwelling velocities in windrows as a function of wind speed for a given mixing depth (here, 40 m). Unsurprisingly, the maximum is located near (but not necessarily at) the middle of the mixed layer. As the wind increases, the depth of the maximum deepens asymptotically to the midpoint of the mixed layer.

Figure 7-

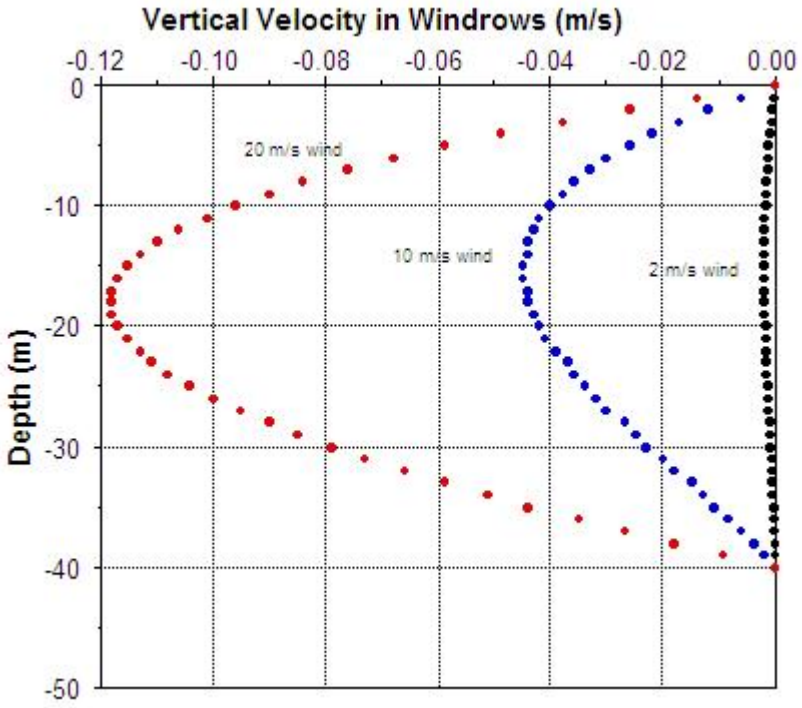

Figure 8 shows the same behavior as that in the preceding figure, except in terms of wavelength. An increase in peak wavelength causes the maximum downwelling to deepen.

Figure 8-

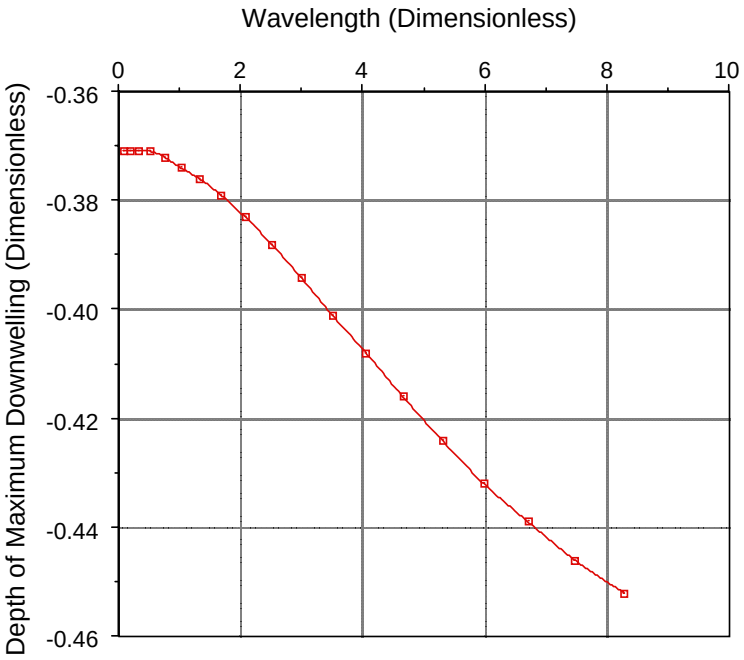

Figure 9 shows the effects of increasing winds for different mixed layer depths.

Figure 9-

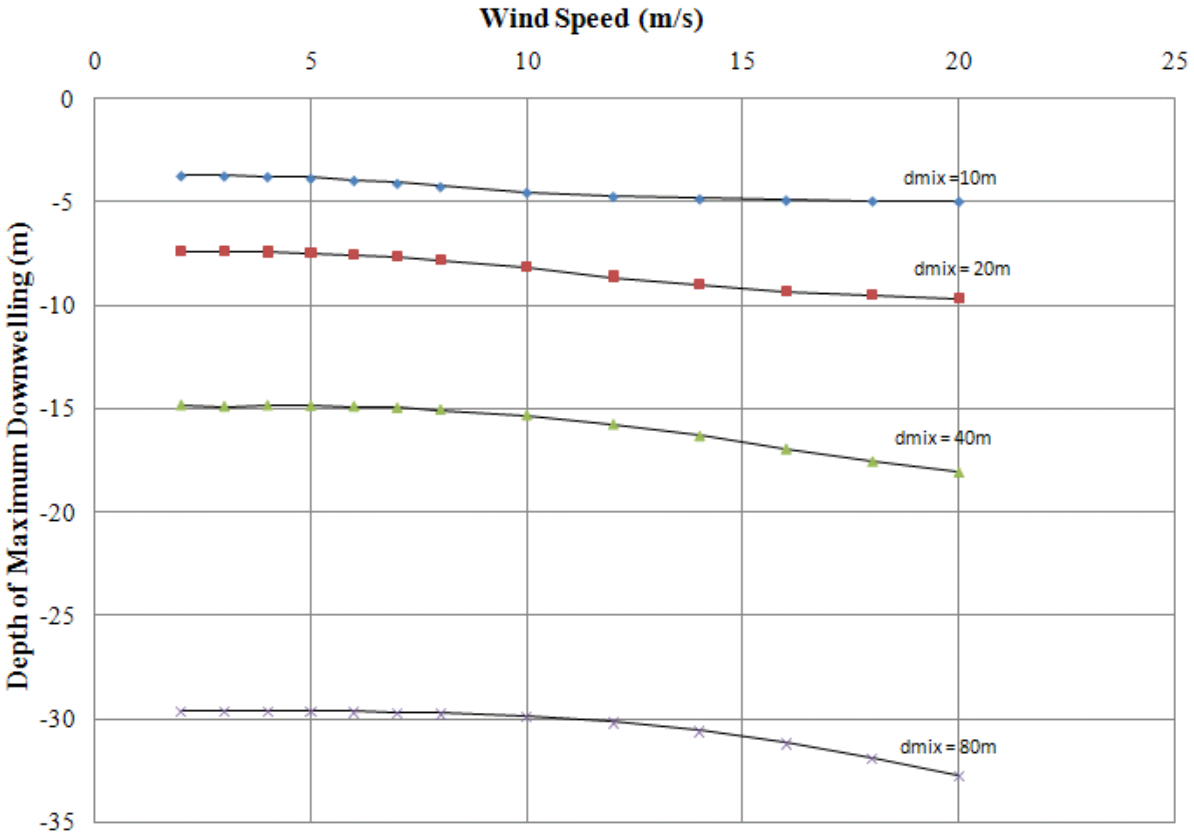

Referring to the downwelling equation (2.9), clearly, r serves as an important "switch" that turns Langmuir circulation "on" or "off", depending on the wave spectrum. Figure 10 suggests that Langmuir circulation continues to operate down to very low wind speeds.

Figure 10-

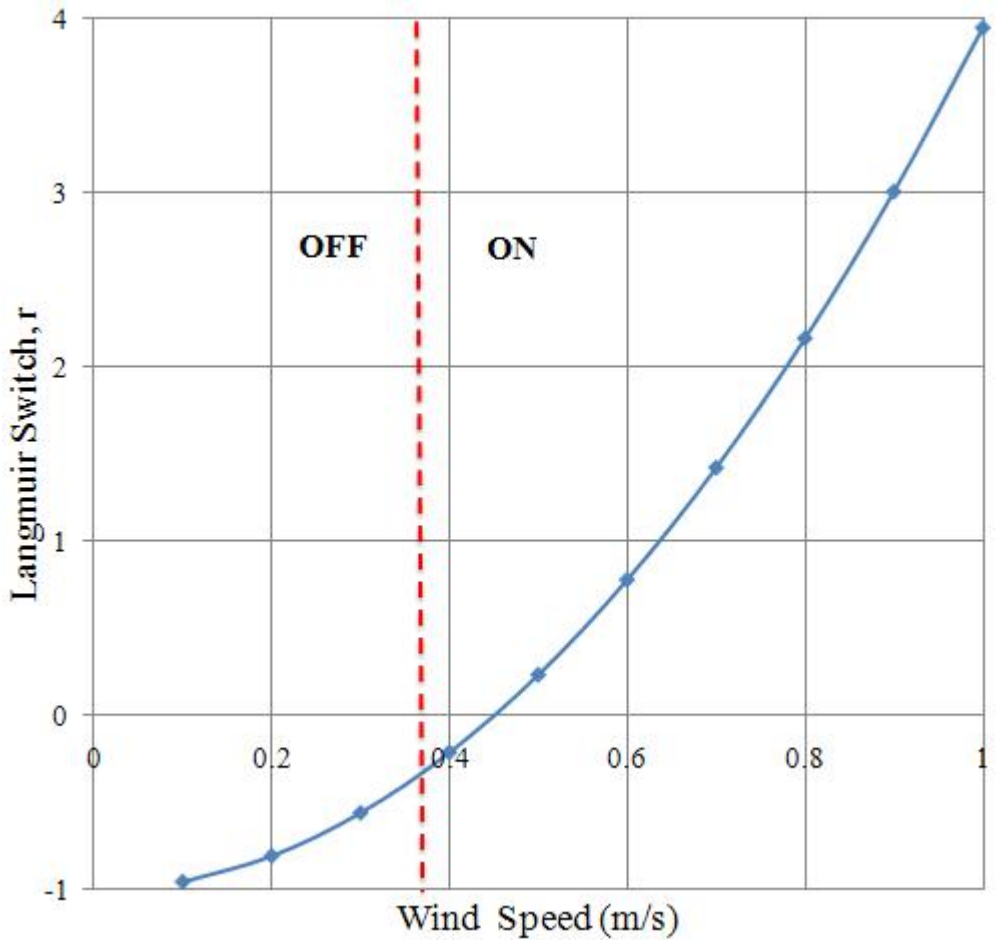

The downwind Langmuir circulation exhibits jet-like behavior at the surface convergences, where oil is collected and moves downwind with a characteristic value of the jet maximum. OILTRACK calculates the sum of the horizontal average downstream speed and the maximum jet occurring at the convergences.

$$\boldsymbol{U}_{LC} = \langle \boldsymbol{U}_{LC} \rangle + \boldsymbol{U}_{LC_{jet}} \qquad (2.13)$$

The average is taken to be

$$\langle U_{LC} \rangle = 0.022 U_{10} . \qquad (2.14)$$

OILTRACK fits the jet by

$$U_{LC_{jet}} = u_* R_* \sqrt{r} \left[0.4 e^{-0.278} + \frac{1}{0.459r + 2.3879\sqrt{r} + 0.7515} \right] \qquad (2.15)$$

Figure 11-

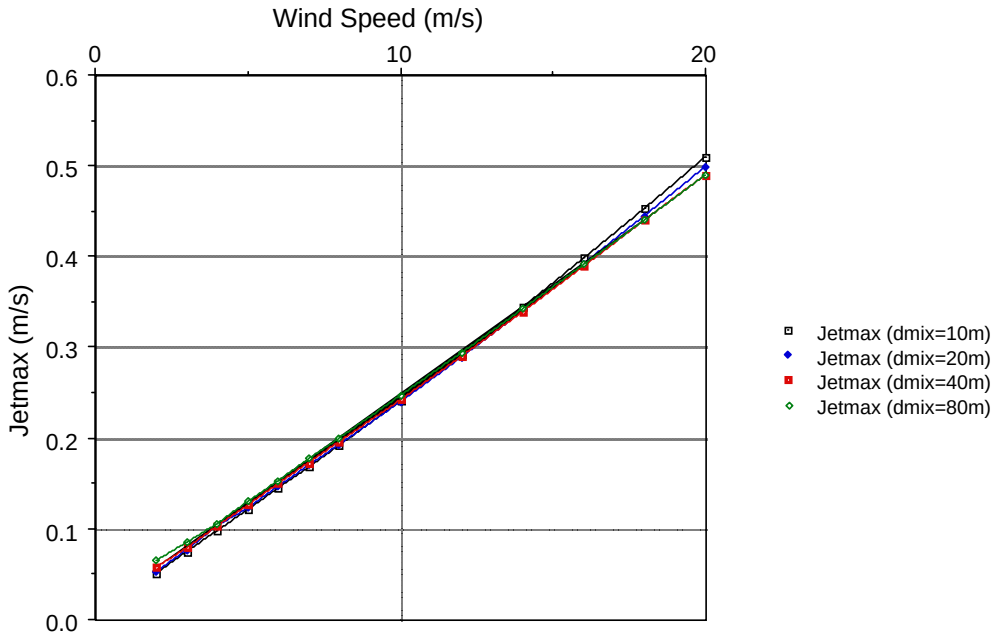

Figure 11 shows the expected result that the maximum jet is directly proportional to the wind speed, regardless of the mixing depth.

The lateral speed $V_s(y)$ at which Langmuir cells sweep water into convergences is approximately sinusoidal.

$$V_s(y) = V_{max} \sin\left(\frac{2\pi}{L_s}(y - y_c)\right) \qquad (2.16)$$

A maximum occurs at the cell center and a convergence at y_c.

Where

$$V_{max} = 6.07\sqrt{\frac{Ra - Ra_c(\kappa)}{Ra_c(\kappa)}} \qquad (2.17)$$

Figure 12-

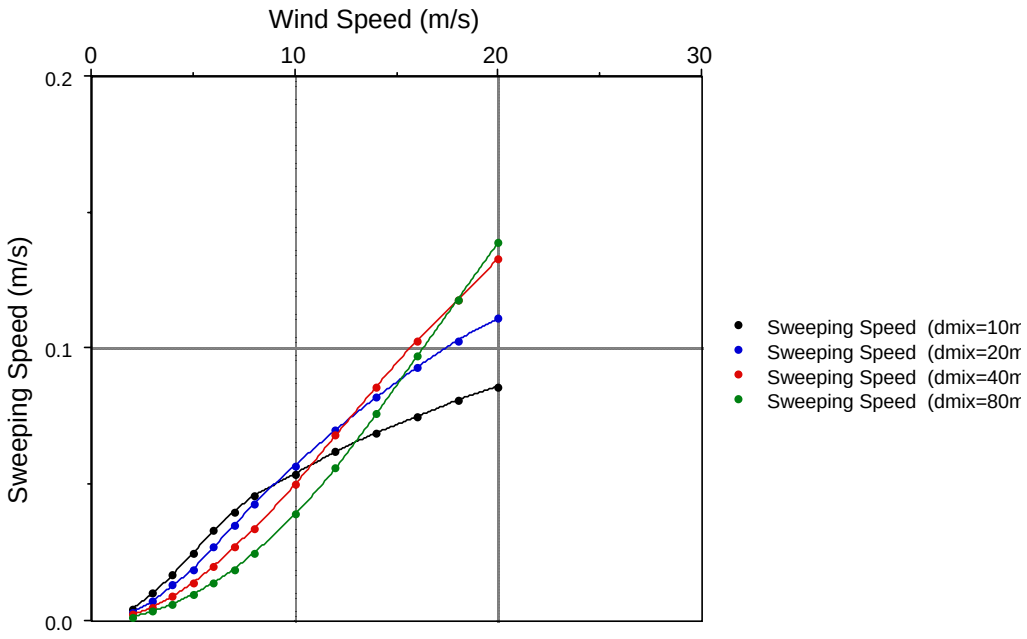

OILTRACK estimates the steady-state, fractional amount of oil that has been swept into windrows by: (1) balancing net lateral shear stress at the oil-water interface with the hydrostatic pressure variation in the oil and (2) conserving volume of oil at the surface.

OILTRACK assumes that spilled oil moves with the sum of the following surface vectors:

$$U_{oil}(x,y,t) = U_c(x,y,t) + \left\{\overline{U}(x,y,t) + u_{s(0)}(x,y,t)\right\}, \qquad (2.18)$$

where

$U_c(x,y,t)$ is the prescribed surface current.

$\overline{U}(x,y,t)$ is the *mass-weighted* average of the downwind surface current.

$u_{s(0)}(x,y,t)$ is the surface Stokes drift.

The definition of $\overline{U}(x,y,t)$ requires an important explanation, hence the following derivation:

The horizontal components of the depth-averaged Navier-Stokes equations for the layer of oil of thickness $\boldsymbol{h(x,y,t)}$ are

$$\frac{\partial h\bar{u}}{\partial t} + \frac{\partial h\overline{uu}}{\partial x} + \frac{\partial h\overline{uv}}{\partial y} = \chi g h \frac{\partial h}{\partial x} + \frac{\tau_x}{\rho_o}, \qquad (2.19)$$

$$\frac{\partial h\bar{v}}{\partial t} + \frac{\partial h\overline{uv}}{\partial x} + \frac{\partial h\overline{vv}}{\partial y} = \chi g h \frac{\partial h}{\partial y} + \frac{\tau_y}{\rho_o}, \qquad (2.20)$$

$$\frac{\partial h}{\partial t} + \frac{\partial h\bar{u}}{\partial x} + \frac{\partial h\bar{v}}{\partial y} = 0, \qquad (2.21)$$

where τ_x and τ_y are the depth-averaged horizontal stresses in the oil layer.

If the oil velocity is assumed to be independent of $\boldsymbol{x}$, then the above equations are:

$$\frac{\partial h\bar{u}}{\partial t} + \frac{\partial h\overline{uv}}{\partial y} = \frac{\tau_x}{\rho_o}, \qquad (2.22)$$

$$\frac{\partial h\bar{v}}{\partial t} + \frac{\partial h\overline{vv}}{\partial y} = \chi g h \frac{\partial h}{\partial y} + \frac{\tau_y}{\rho_o}, \qquad (2.23)$$

$$\frac{\partial h}{\partial t}+\frac{\partial h\bar{v}}{\partial y}=0 \qquad (2.24)$$

A quasi-steady-state requires that $h\bar{v}$ be constant, and since $\bar{v}$ must be zero for some value of y, $\bar{v}$ must be zero for all values of y. Hence, the x-component of the net shear stress in the oil is zero, i.e., $\tau_x = 0$. So, Equations (2.22 – 2.24) just become

$$\chi g h\frac{\partial h}{\partial y}+\frac{\tau_y}{\rho_o}=0 \qquad (2.25)$$

Equation (2.25) simply shows a balance between the hydrostatic pressure of the oil and the net lateral shear stress on the oil. So, in principle, Equation (2.25) can now be solved for the oil thickness.

$$h(y)=\sqrt{\left(\frac{2}{g\chi}\int_{y_o}^{y}\frac{\tau_y}{\rho_o}dy\right)}, \qquad (2.26)$$

where $0 < y_o$ is the part of the Langmuir cell that has been swept of oil.

The stress is taken to be

$$\frac{\tau_y}{\rho_o}=C_D\frac{\rho_w}{\rho_o}|V_w|V_w, \qquad (2.27)$$

where V_w is the water velocity at the water-oil interface (which is essentially the same as the sweeping velocity).

From equations (2.16-2.27) oil thickness becomes

$$\frac{h(\eta)}{h_0} = \sqrt{\Gamma}\left[\eta - \eta_0 - \frac{1}{\pi}\cos(\eta + \eta_0)\sin(\eta + \eta_0)\right] \quad (2.28)$$

where

$$\Gamma = C_D \frac{\rho_w}{\rho_o} \frac{L_s^{\,2}}{h_o^{\,2}} \frac{U_{LC}^{\,2}}{\chi g L_s} \quad (2.29)$$

$$\chi = \frac{\rho_w - \rho_o}{\rho_w},$$

$$\int_{\eta_o}^{1} \frac{h(\eta)}{h_0} d\eta = 1 \quad (2.30)$$

h_o is a *user-specified*, initially uniform oil thickness, and η_o is chosen to assure that surface oil volume is conserved, keeping in mind that oil has been swept "clean" for $\eta_0 \le 0$. Combining Equations (2.28-2.30) allows the evaluation of η_o:

$$\eta_o = \left(1 - 0.844\Gamma^{\frac{-1}{5}}\right) \quad (2.31)$$

Finally, Equation (2.31) is used to define $\overline{\boldsymbol{U}}(\boldsymbol{x},\boldsymbol{y},\boldsymbol{t})$ in Equation (2.18)

$$\overline{U}_{LC} = \frac{1}{L_s h_0}\int_0^{L_s} h(y) U_{LC}(y) dy, \quad (2.32)$$

Figures 13 - 15 demonstrate the efficacy of Langmuir circulation in sweeping spilled oil into windrow convergences.

(Note that the coefficient 0.844 in Equation (2.31) corrects OILTRACK's original value of 0.735. The resulting difference between the two coefficients is trivial.)

Figure 13-

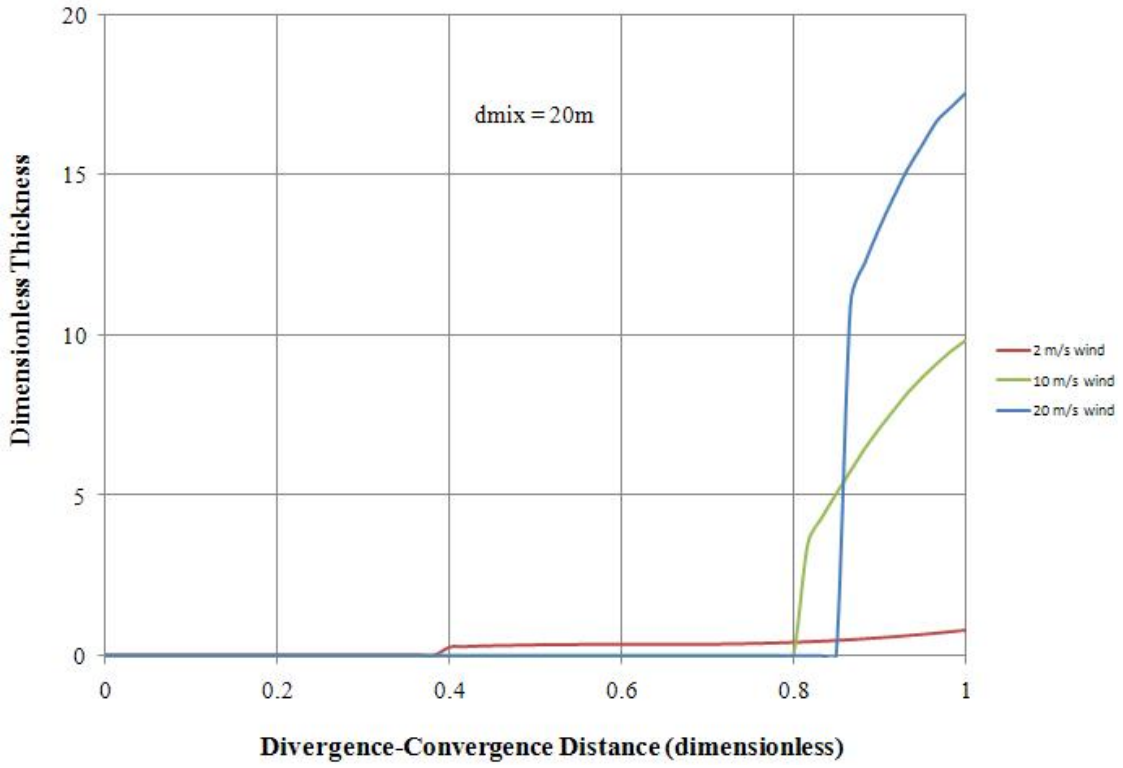

Figure 14-

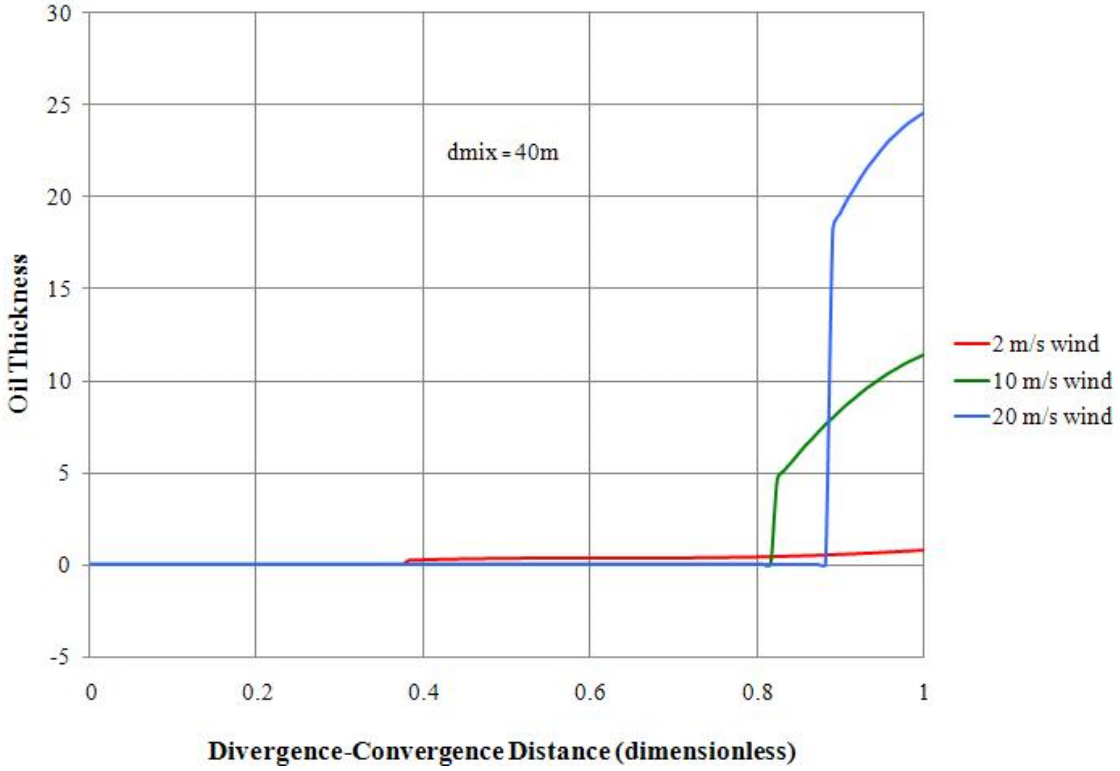

Figure 15-

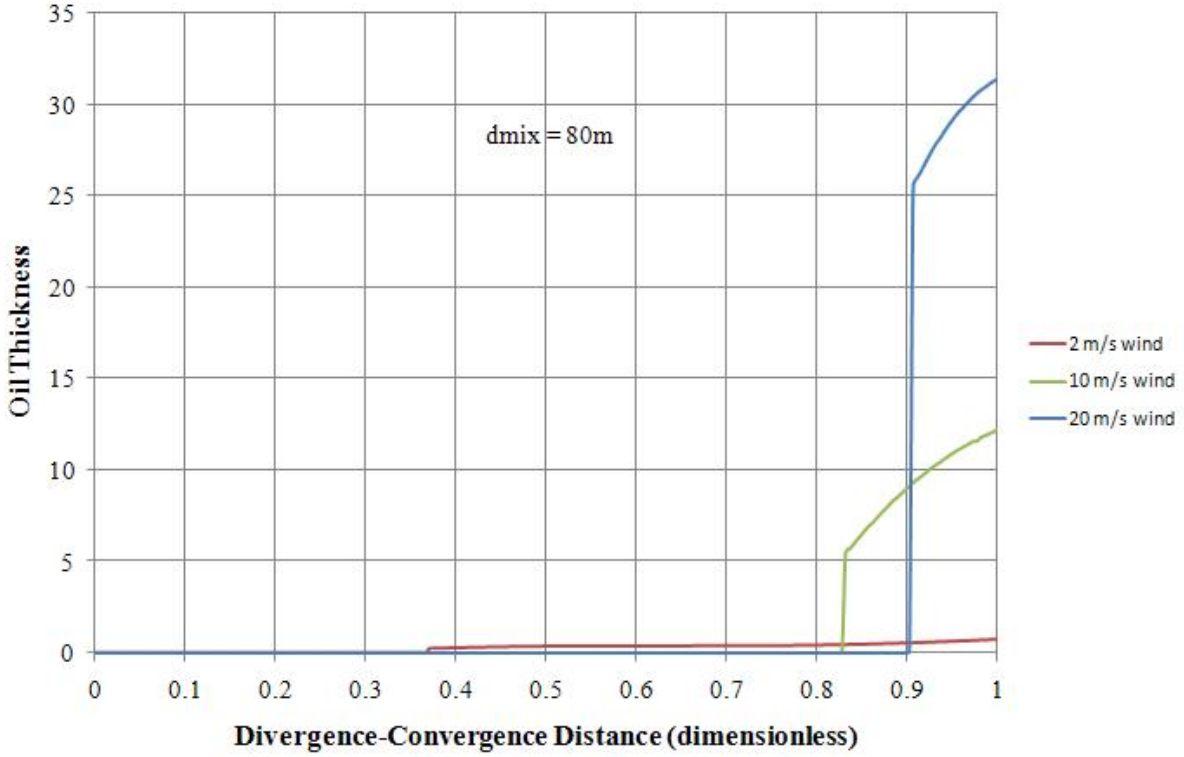

From a spill responder's point of view, one of the most practical considerations is the oil thickness at Langmuir convergences: in other words, the *endpoints* (maximal values) of Figures 13 - 15 relative to *initial* spill thickness. Figures 16 - 18 present such estimations for a range of wind conditions and oil densities.

Figure 16-

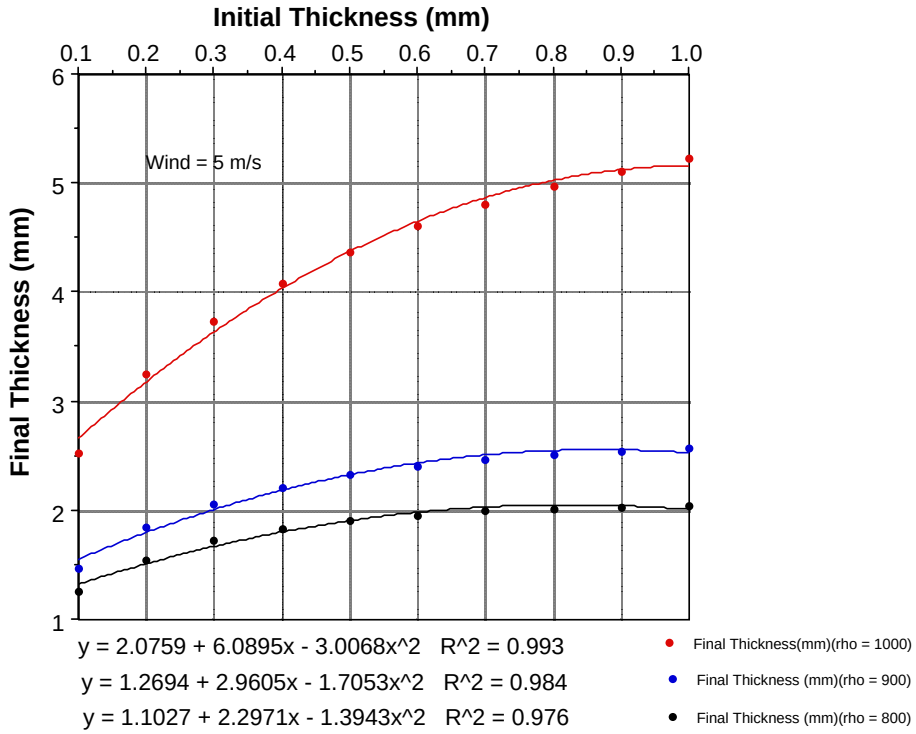

Figure 17-

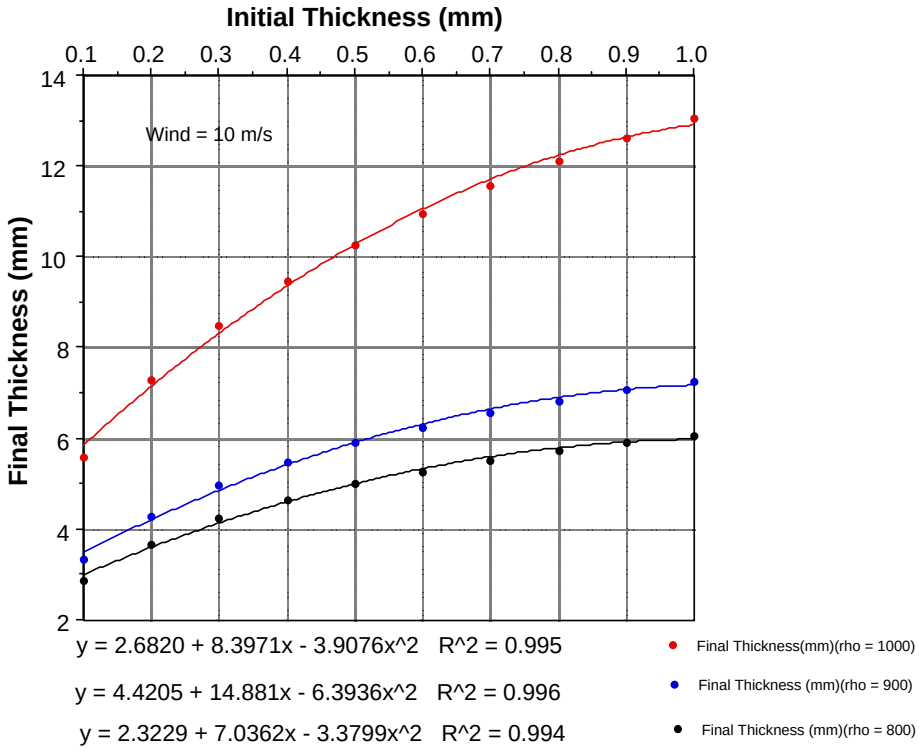

Figure 18-

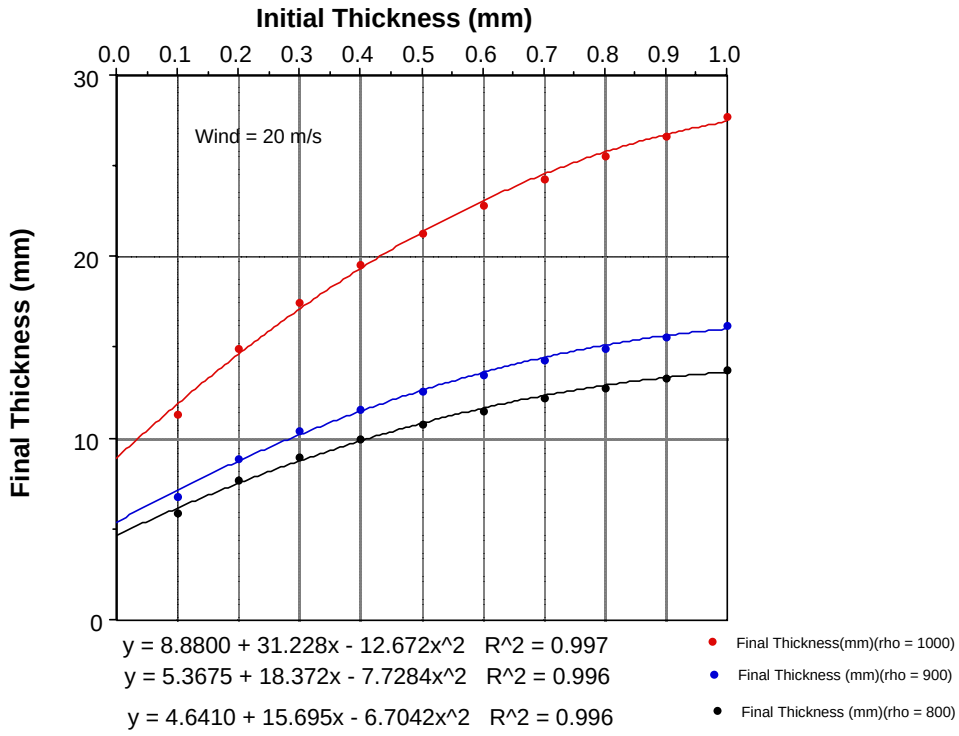

The immediate observation of Figures 16 - 18 confirms the fact that, for any given wind and oil density, the final slick thickness is a quadratic function of its initial thickness.

The bottom line is that under most conditions of wind- and windrow-spacing, spilled oil could collect in convergences comprising only 20%, or less, of the original spills' area. (Note: The 2 m/s graph is unreliable.) However (not shown in these graphs), the results for a 5 m/s wind suggest that oil could still be swept to within 25% of the original area).

A practical question should be raised here: Since this version of OILTRACK is basically steady state, it is not surprising that most of the wind/mixed-layer scenarios come to roughly the same conclusions on a percentage basis. However, as windrow spacing increases, for a given wind and mixed layer depth, obviously the terminal sweeping time correspondingly increases. So, when OILTRACK is used in a time-dependent mode simulation time-steps should be greater that the sweeping time for the dominant windrow spacing.

Figures 19 - 20 show the same results in slightly different forms.

Figure 19-

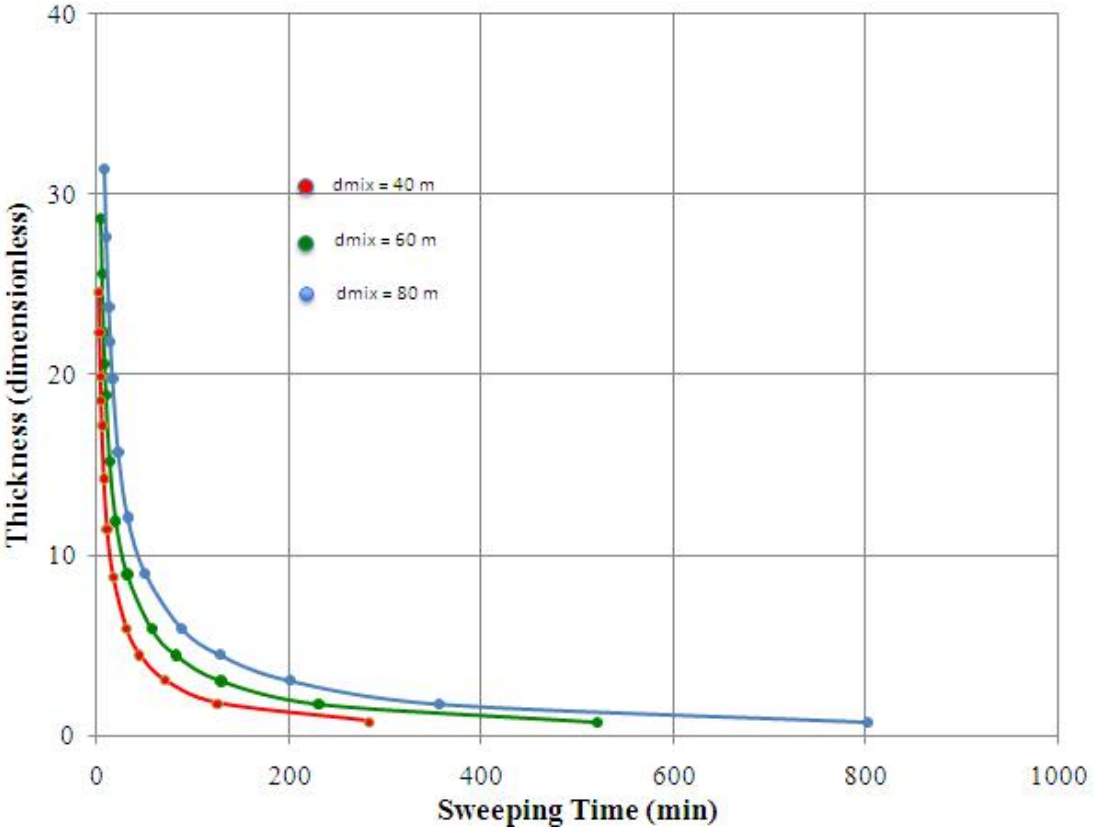
40
30
20
10
0
Thickness (dimensionless)
dmix = 40 m
dmix = 60 m
dmix = 80 m
0
200
400
600
800
1000
Sweeping Time (min)

Figure 20-

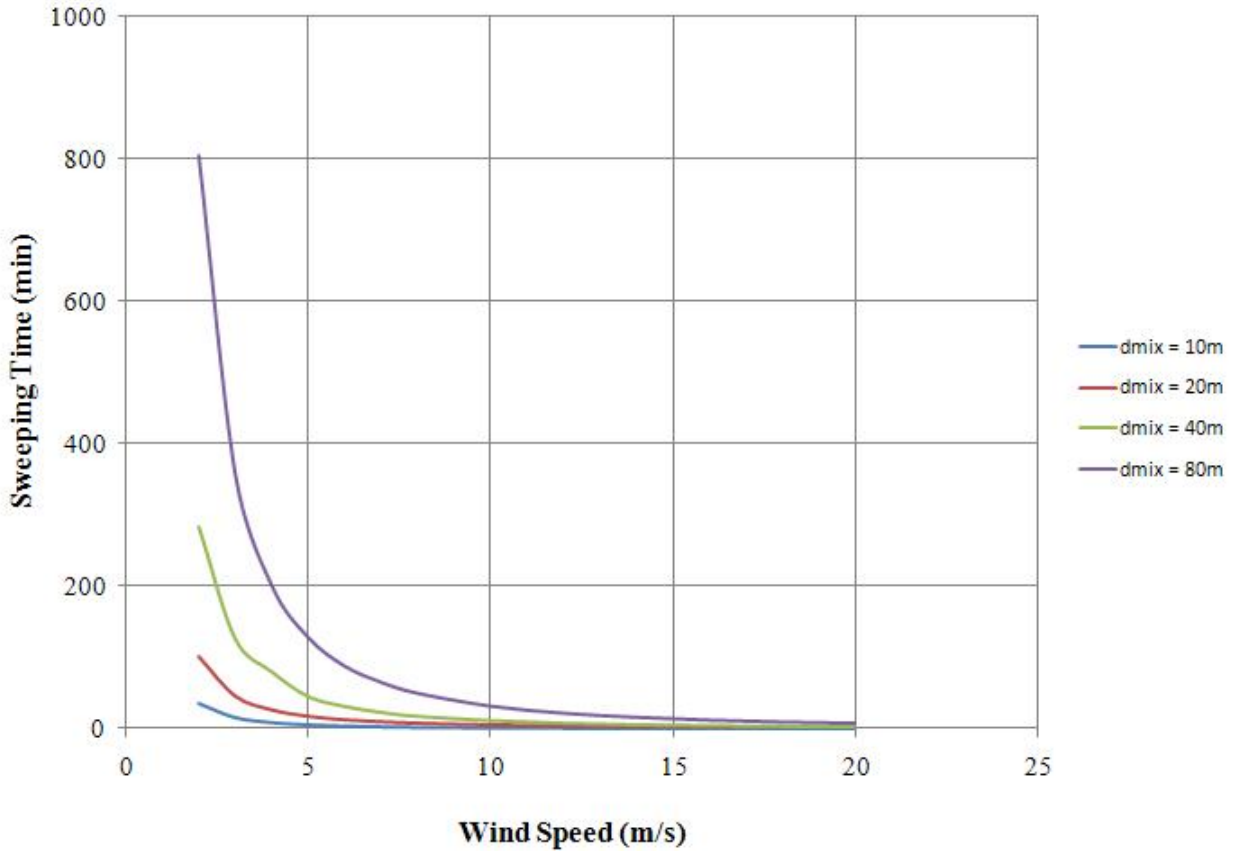

OILTRACK uses the following experimental expression for the terminal velocity $\boldsymbol{V_T}$ of buoyant oil droplets.

$$V_T = 1.35\left[\sqrt{\frac{2ag}{3}\frac{\Delta\rho}{\rho}} - \frac{11.53\nu}{a}\right], \qquad (2.33)$$

where

$\frac{\Delta\rho}{\rho}$ is the fractional difference between oil and water density,

$\boldsymbol{a}$ is the droplet radius, and $\boldsymbol{\nu}$ is the viscosity of water.

Equation (2.4) is a slight correction to the commonly used Stokes equation by accounting for the viscosity of water as a droplet rises.

The Stommel (1949) retention zone (SRZ) is found by a balance of the buoyant droplet velocity and the Langmuir downwelling velocity. So, for a given droplet size the retention depth is found to be the largest root of

$$w(z) + V_T = 0 . \qquad (2.34)$$

2.3 Discussion:

There is now sufficient experimental and theoretical evidence to conclude that Langmuir circulation is a ubiquitous phenomenon, and that this process is an important agent for turbulence and convective motions in the mixed layer. Now that the importance of Langmuir circulation is becoming more widely appreciated, other less obvious evidence of this type of motion is being reported. For instance, Kempema and Dethleff (2006) report the results of acoustic Doppler current measurements in a lake containing frazil ice. They found slush ice in windrows on the lake surface. Further examination of ice samples showed that it contained more bottom sediments in the ice beneath convergences than that in the upwelling areas between windrows.

Finally, Figure 21 shows distinct windrows in a somewhat analogous process to that discussed above. In this case, however, the Langmuir circulation was observed in the extraordinarily clear, shallow (4-5m) waters of the Bahamas Banks.

Figure 21-

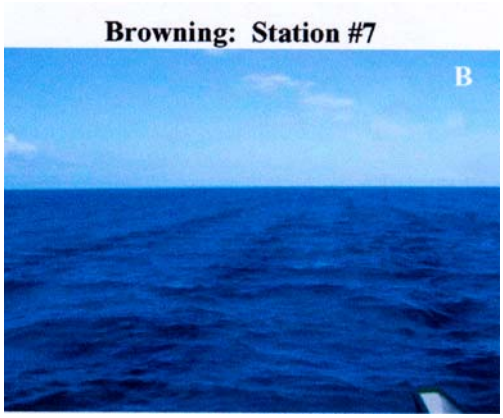

From Dierssen et al (2004)

The presence of Langmuir circulation is very clear. In this case, however, the "windrows" are on the bottom, rather than on the surface. Using a tethered buoy containing optical instruments, Dierssen et al (2004) were able to detect rows of benthic algae aligned with the wind and alternating with clean sand. In other words, the Langmuir circulation swept the algae into windrows on the bottom.

OILTRACK has a number of shortcomings, some of which might be partially corrected in the future. For example, it does not model windrows' observed evanescence, migration, and blending. The presence of these features are both observed in the field and predicted by large eddy simulations (LES) of Langmuir circulation. Of course, the latter are impractical for operational use. However, it might be possible to use quasi-time-dependent envelopes of OILTRACK, based on the present knowledge that windrows' lifetimes are lognormally distributed, as discussed by Overstreet (2005). Another example that might be explored is the use of the JONSWAP formulation for the spectral peak and Stokes drift for developing seas, since it is included here. However, this "improvement", while mathematically feasible, might not be

particularly meaningful, since OILTRACK's correlation functions were based on statistics for fully developed waves.

References:

Craik, A.D.D. and S. Leibovich, "A Rational Model for Langmuir Circulations", *Journal of Fluid Mechanics*, **73**, 401-426, 1976.

Dierssen, H.M, R. C. Zimmerman and D. Bridge, "Wind rows and Whiting: Unique Bio-Optical Phenomenon in the Bahamas Banks", *Proc. Ocean Optics XVII* , 2004.

Delvigne, G.A. and C.E. Sweeny, "Natural Dispersion of Oil", *Oil and Chemical Pollution*, **4**, 281-310, 1988.

Kempema, E.W. and D. Dethleff, "The Role of Langmuir Circulation in Suspension Freezing", *Annals of Glaciology*, **44**(1), 58-62, 2006.

Large, W.G. and S. Pond, "Open ocean momentum flux measurements in moderate to strong winds", *Journal of Physical Oceanograph*y. **11**, 324-336, 1981.

Leibovich, S, "The form and dynamics of Langmuir Circulations", *Annual Review of Fluid Mechanics*, **15**, 391-427, 1983.

Leibovich, S, "Surface, and near-surface motion of oil in the sea", Final Report. Contract 14-35-0001-30612 Mineral Management Service, Department of Interior, 1997.

Leibovich, S. and S. Paolucci, "Energy stability of the Eulerian-mean motion in the upper ocean to three-dimensional perturbation", *Physics of Fluids*, **23**(7), 1980.

Marmorino, G., "Infrared imagery of large-aspect-ratio Langmuir circulation", *Continental Shelf Research,* **25**(1), 1-6, 2005.

Overstreet, R., "Parameterization of Dispersion in the Mixed Layer: Turbulence and Langmuir Circulation", NOAA, HMRD Report, Purchase Order # AB133C-03-SE-1171, 2005.

Skyllingstad, E.D. and W.D. Denbo, "An ocean large-eddy simulation of Langmuir circulations and convection in the surface mixed layer", *Journal of Geophysical Research*, **100**, 8501-8522, 1995.

Smith, J. R.Pinkel and R.Weller, "Vertical structure in the mixed layer during MILDEX", *Journal of Physical Oceanograph*y, **17**, 425-439, 1987.

Stommel, H., "Trajectories of small bodies sinking slowly through convection cells", *Journal of Marine Research*, **8**, 24-29, 1949.

Szeri, A.J., "Langmuir Circulation on Rodeo Lagoon", *Monthly Weather Review"*, **124**(2), 341-342, 1996.

Thorpe, S.A., "Langmuir circulation", *Annual Review of Fluid Mechanics,* **36**, 55-79, 2004.

Weller, R.A. and J.F. Price, "Langmuir circulation within the oceanic mixed layer", *Deep-Sea Research*, **35**(5), 711-747, 1988.

Zedel, L. and D. Farmer, "Organized structures in subsurface bubble clouds: Langmuir circulation in the open ocean", *Journal of Geophysical Research*, **96**:C5, 8889-8900, 1991.